

Symmetry Breaking and Bifurcations in the Periodic Orbit Theory: II | Spheroidal Cavity |

Alexander G. M agner,^{a,b,c} Ken-ichiro Arita,^d Sergey N. Fedotkin^{b,c}
and Kenichi Matsuyanagi^e

^aResearch Center for Nuclear Physics, Osaka University, Osaka 567-0047, Japan

^bInstitute for Nuclear Research, 03680 Prospekt Nauki 47, Kiev 28, Ukraine

^cInstitute for Theoretical Physics, University of Regensburg, D-93040 Regensburg,
Germany

^dDepartment of Physics, Nagoya Institute of Technology, Nagoya 466-8555, Japan

^eDepartment of Physics, Graduate School of Science, Kyoto University,
Kyoto 606-8502, Japan

We derive a semiclassical trace formula for the level density of the three-dimensional spheroidal cavity. To overcome the divergences and discontinuities occurring at bifurcation points and in the spherical limit, the trace integrals over the action-angle variables are performed using an improved stationary phase method. The resulting semiclassical level density oscillations and shell energies are in good agreement with quantum-mechanical results. We find that the births of three-dimensional orbits through the bifurcations of planar orbits in the equatorial plane lead to considerable enhancement of shell effect for superdeformed shapes.

x1. Introduction

The periodic orbit theory (POT)^{1){10}} is a nice tool for studying the correspondence between classical and quantum mechanics and, in particular, the interplay of deterministic chaos and quantum-mechanical behavior. But also for systems with integrable or mixed classical non-linear dynamics, the POT leads to a deeper understanding of the origin of shell structure in finite fermion systems such as nuclei,^{8),11){13}} metallic clusters,^{14){16}} and mesoscopic semiconductors.^{17){21}} Bifurcations of periodic orbits may play significant roles, e.g., in connection with the superdeformations of atomic nuclei,^{8),9),12),22){24}} and were recently shown to affect the quantum oscillations observed in the magneto-conductance of mesoscopic devices.^{19),20}} This phenomenon is observed for some control parameters (shapes, magnetic field etc.) of the potential well, for which the orbits bifurcate and new type of periodic orbits emerge from the original ones. Examples can be found, e.g., in elliptic billiard and spheroidal cavity.^{8),9),12),23){28}} In elliptic billiard, short diametric orbits with repetitions bifurcate at certain values of deformation parameter, and new orbits with hyperbolic caustics (butterfly-shaped orbit etc.) emerge from them. In spheroidal cavity, periodic orbits in the equatorial plane bifurcate, and new three-dimensional orbits emerge.

The semiclassical trace formulae connect the quantum-mechanical density of states with a sum over the periodic orbits of the classical system.^{1){4}} In these for-

mulae, divergences arise at critical points where bifurcations of periodic orbits occur or where symmetry breaking (or restoring) transitions take places. At these points, the standard stationary phase method (SSPM),¹⁾ used in the semiclassical evaluation of the trace integrals, breaks down. Various ways of avoiding these divergences have been studied,^{3),5),29)} some of them employing uniform approximations.^{29),(37)} Here we employ an improved stationary-phase method (ISPM) for the evaluation of the trace integrals in the phase-space representation, which we have derived for the elliptic billiard²⁸⁾ and very recently for the spheroidal cavity.²⁴⁾

The singularities of the SSPM near the bifurcation points are due to the peculiarities of its asymptotic expansions. In the ISPM,^{24),28)} the catastrophe integrals^{38),39)} are evaluated more exactly within the finite integration limits in the phase-space trace formula,^{3),5),9),24),28),40)} and one can overcome the singularity problem due to bifurcations, which occur when the stationary points lie near the ends of the integration region in the action-angle variables. We can also take into account the stationary points outside the classically accessible region ("ghost orbits").⁵⁾ This method is particularly useful for integrable systems where integration limits are easily obtained. This theory has been developed in Ref. 28) for the case of the bifurcations through which periodic orbit families with maximal degeneracy emerge from the orbits with smaller degeneracy. The essential difference between our method presented in this paper and that with the uniform approximation of Refs. 32) and 35) is that we improve the calculation of the angle part of the phase-space trace integral for the orbits with smaller degeneracies. Taking the elliptic billiard as an example, we have applied the ISPM to the integration over the angle variable for short diametric orbits, and derived the improved trace formula which is continuous through all bifurcation points including the circular limit and the separatrix. We have then shown that significant enhancements of the shell effect in level densities and shell structure energies occur at deformations near the bifurcation points. Away from the bifurcation points, our result reduces to the extended Gutzwiller trace formula,^{4),8),(10)} and for the leading-order families of periodic orbits, it is identical to that of Berry and Tabor.⁵⁾

The main purpose of this paper is to extend our semiclassical ISPM to the three-dimensional (3D) spheroidal cavity,²⁴⁾ which may be taken as a simple (highly idealized) model for a heavy deformed nucleus^{8),11)} or a deformed metallic cluster,^{14),15)} and to specify the role of periodic orbit bifurcations in the shell structure responsible for superdeformations. Although the spheroidal cavity is integrable, it exhibits all the difficulties mentioned above (i.e., symmetry breaking and bifurcations) and therefore gives rise to an exemplary case study of a non-trivial 3D system. We apply the ISPM for the bifurcating orbits and succeed in reproducing the superdeformed shell structure by the POT, hereby observing a considerable enhancement of the shell effect near the bifurcation points.

¹⁾ In this paper SSPM denotes the standard stationary phase method and its extension to continuous symmetries.^{3),(5),7)}

x2. Classical mechanics for the spheroidal cavity

The semiclassical trace formulas for the oscillating part of the level density for the spheroidal cavity are determined by the characteristic properties of the classical periodic families.^{(8), (9), (22), (27)} This section is an outlook of the definitions and solutions of the classical mechanics for the spheroidal cavity in line of Refs. (8), (9), (23) and (27). They will be used for the semiclassical derivations of the trace formulas improved at the bifurcation points. We shall pay special attention to the 3D periodic orbits which emerge through bifurcations and play important roles as the semiclassical origin of superdeformed shell structure.^{(8), (23), (27)}

2.1. General periodic-orbit formalism

We characterize the spheroid by its ratio of semi-axes b/a keeping its volume fixed, and consider the prolate case with $b/a > 1$, where the major axis coincides with the symmetry axis. We first transform the Cartesian coordinates $(x; y; z)$ into the usual cylindrical coordinates $(\rho; \phi; z')$, where $\rho = \sqrt{x^2 + y^2}$, which are expressed in terms of the spheroidal coordinates $(u; v; \phi')$

$$\rho = a \cosh u \sinh v; \quad z = a \sinh u \cosh v; \quad \phi = \phi' \frac{b^2 - a^2}{a^2} \quad (2.1)$$

with

$$-\frac{\pi}{2} \leq u \leq \frac{\pi}{2}; \quad 0 \leq v < 1; \quad 0 \leq \phi' < 2\pi. \quad (2.2)$$

The values of u define the positions of the foci of the spheroid lying on the z -axis. Taking into account the volume conservation condition $a^2 b = R^3$, one has $b = R^{2/3}$ and $a = R^{1/3}$. As is well known, the Hamilton-Jacobi equations separate in the coordinates $(u; v; \phi')$ for the spheroidal cavity.

In the Hamilton-Jacobi formalism, classical dynamics is determined by the partial actions. In the spheroidal coordinates these are given by

$$I_u = \frac{p}{2\pi} \int_{u_c}^{u_c} du \sqrt{1 - \sin^2 u \frac{2}{\cos^2 u}}; \quad (2.3a)$$

$$I_v = \frac{p}{2\pi} \int_{v_b}^{v_b} dv \sqrt{\cosh^2 v - 1 - \frac{2}{\sinh^2 v}}; \quad (2.3b)$$

$$I_\phi = \int_{\phi_c}^{\phi_c} d\phi = p \frac{\phi_c}{2}; \quad (2.3c)$$

where $\frac{p}{2\pi} \int_{\phi_c}^{\phi_c} d\phi$ is the projection of the angular momentum onto the symmetry axis, and $p = \sqrt{2mE}$, m is the particle mass. In Eqs. (2.3) we introduced new "action" variables I_1 and I_2 related to the turning points u_c, u_c and v_c, v_b along the trajectory in the $(u; v)$ coordinates; $u = u_c$ and $v = v_c$ are the (hyperbolic and elliptic) caustic surfaces,

$$\cosh v_c = \left(\frac{1}{2} (1 + I_1) + \frac{1}{4} (1 - I_1)^2 + I_2 \right)^{1/2}; \quad (2.4a)$$

$$\sin u_c = \frac{1}{2}(1 + \epsilon_1) - \frac{1}{4}(1 - \epsilon_1)^2 + \epsilon_2^{1=2} \epsilon_1^{1=2}; \quad (2.4b)$$

and $v = v_b$ is the spheroid boundary, given by $\cosh v_b = \frac{p}{2} - 1$. The condition that the kinetic energy must be positive determines the limits for the variables ϵ_1 and ϵ_2 ,

$$\begin{aligned} \epsilon_1 &= \epsilon_2 - \epsilon_1 - \frac{\epsilon_2^2}{2 - \epsilon_1} - \epsilon_2^2 - \epsilon_1 = \epsilon_1^+; \\ \epsilon_2 &= 0 - \epsilon_2 - \frac{1}{2 - \epsilon_1} = \epsilon_2^+; \end{aligned} \quad (2.5)$$

These inequalities together with 2π intervals for the corresponding angle variables determine the tori of the classically accessible motion with the boundaries $\epsilon_1(\epsilon_2)$ and ϵ_2 .

According to Eqs. (2.3), the particle energy E is a function of only the action variables I_u, I_v and I_ϕ , $E = H(I_u; I_v; I_\phi)$ due to integrability of the system under consideration. These relations define the partial frequencies ω_u, ω_v and ω_ϕ through $\omega_j = \partial H / \partial I_j$. The periodicity conditions for the classical trajectories are significantly simplified in terms of the partial frequencies ω_j . Introducing the new variables θ and ϕ ,

$$\theta = \frac{\sin u_c}{\cosh v_c}; \quad \phi = \arcsin \frac{\cosh v_c}{\cosh v_b}; \quad (2.6)$$

along with the energy E instead of the partial actions I_u, I_v and I_ϕ (or ϵ_1 and ϵ_2), they read

$$\frac{\omega_u}{\omega_v} = \frac{1}{2} - \epsilon_1 - \frac{F(\epsilon_1; \epsilon_2)}{F(\epsilon_1)} = \frac{n_u}{n_v}; \quad (2.7a)$$

$$\begin{aligned} \frac{\omega_\phi}{\omega_u} &= \frac{2}{\epsilon_1} - \epsilon_1 - \epsilon_2^{1=2} - \epsilon_1 - \epsilon_2^{1=2} - \epsilon_2^{1=2}; \quad F(\epsilon_1) \\ &+ \epsilon_2^2; \quad \epsilon_1^2; \quad \epsilon_1 \frac{F(\epsilon_1; \epsilon_2)}{F(\epsilon_1)} = \frac{n_\phi}{n_u}; \end{aligned} \quad (2.7b)$$

Here, n_u, n_v and n_ϕ are co-prime integers, $n_u = 1; 2; \dots$; $n_v = 2n_u; n_v = 2n_\phi; n_\phi = 1; 2; \dots$, and $\epsilon_1 = \frac{1}{2} - 1 = (\sin \theta)$. F and E are elliptic integrals of 1st and 3rd kinds (see Appendix A for their definitions). The periodicity condition (2.7) relates $(\epsilon_1; \epsilon_2)$ and $(\epsilon_1; \epsilon_2)$ for a given periodic orbit to the integers n_u, n_v and n_ϕ , which together with the number of repetitions M define this orbit; i.e., $(\epsilon_1; \epsilon_2) = M(n_v; n_\phi; n_u)$.

2.2. Three-dimensional periodic orbits

The 3D periodic orbits (3DPO) $M(n_v; n_\phi; n_u)$ form two-parameter ($K = 2$) families for a given energy E since the number K of free continuous parameters specifying an orbit with fixed energy and the same action is two.^{8),9)} The condition

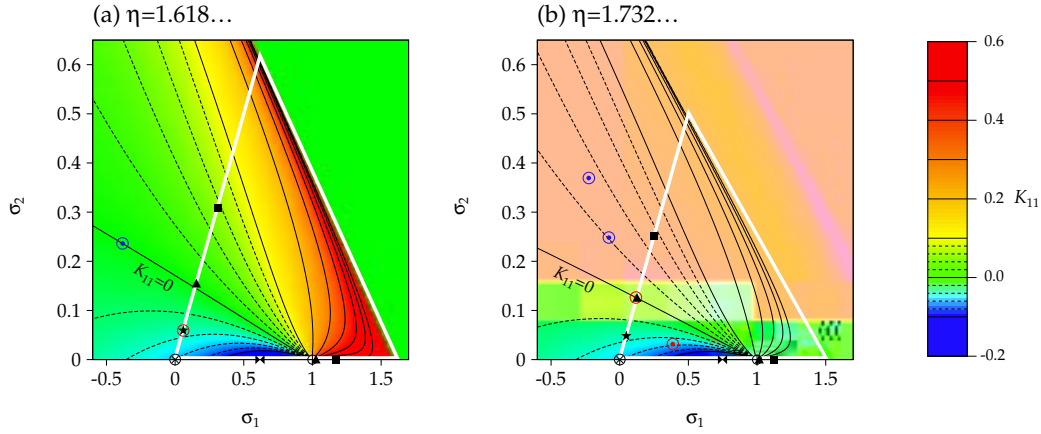


Fig. 1. The triangle of the classically accessible region determined by Eq. (2.5) is indicated by white lines in the $(\sigma_1; \sigma_2)$ plane at bifurcation deformations (a) $\eta = 1.618...$ and (b) $\eta = \sqrt{3}$. The red and blue dots with circles indicate the 3D PO stationary points inside (really existing 3D PO) and outside ("ghost" 3D PO) of this triangle region, respectively. Several examples of the stationary points are indicated: on the $\sigma_2 = 0$ side, the short 2D PO (elliptic triangle, square, and hyperbolic "butterfly"); on the $\sigma_2 = \sigma_1$ side, the short EQ PO (triangle, square, star, and diameter (black crossed circle)). The long diameter (separatrix) is located at $(\sigma_1 = 1; \sigma_2 = 0)$. The color and the contour curves indicate (in unit of $p = 1$) the curvature K_{11} defined by Eq. (3.14).

for 3D PO is the existence of real roots $(\sigma_1; \sigma_2)$ of Eq. (2.7). They appear at the deformation $\eta = \eta_{\text{bif}}$ given by

$$\eta_{\text{bif}} = \frac{\sin(\sigma_{u'} = n_v)}{\sin(\sigma_u = n_v)}; \quad (n_u = 1; 2; \quad \text{or } n_{2n_u} + 1; n_v = 2; 3; \quad) \quad (2.8)$$

where $\sigma_u = 0$ and $\sigma_v = (1 - 2n_u = n_v) = 2$, and exist for larger deformation $\eta > \eta_{\text{bif}}$. These roots determine the caustics (the spheroid $v = v_c$ and the hyperboloids $u = u_c$) of the periodic orbit $M(n_v; n_r; n_u)$ through Eq. (2.6). These caustics are confocal to the boundary of the spheroid $v = v_b$.

Figure 1 shows the stationary points corresponding to the 3D PO for two bifurcation points η_{bif} given by (2.8). The physical tori region (2.5) in the variables σ_i is the triangle. At $\eta_{\text{bif}} = 1.618...$ (Fig. 1a), the stationary point for the 3D PO $(5; 2; 1)$ coincides with that for the star-shaped $(5; 2)$ orbit in the equatorial plane (discussed below) lying on the boundary with $\sigma_2 = \sigma_1$, and moves toward inside of the physical tori region for larger deformations. At $\eta_{\text{bif}} = \sqrt{3}$ (Fig. 1b), the stationary point for the 3D PO $(6; 2; 1)$ lies at the boundary side and coincides with that for triangular orbits in the equatorial plane. At these bifurcation deformations, the lengths of the 3D PO $(5; 2; 1)$ and $(6; 2; 1)$ coincide with those of the star $(5; 2)$ and the doubly repeated triangle $2(3; 1)$,

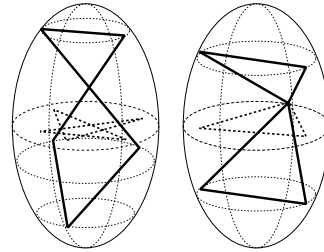


Fig. 2. Short 3D periodic orbits $(5, 2, 1)$ and $(6, 2, 1)$ bifurcated from the equatorial plane orbits $(5, 2)$ and $2(3, 1)$, respectively. Their projections on the equatorial plane are also represented by thick-dashed lines.

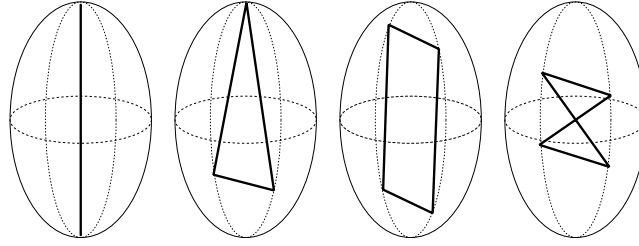


Fig. 3. Some short meridian-plane orbits in the prolate spheroidal cavity: From the left to the right; the isolated long diameter (2;1;1), the elliptic triangular (3;1;1), the elliptic rhomboidal (4;1;1), the hyperbolic "butterfly" (4;2;1).

respectively. Figure 2 illustrates some short 3D PO, and their projections onto the equatorial plane which remind us of the parent equatorial orbits.

2.3. Orbits in the meridian plane

Equation (2.7) have partial solutions for $(\mu_1; \mu_2)$ and $(\mu_1; \mu_2)$ which correspond to the separate families of orbits, i.e. two-dimensional periodic orbits (2D PO), in the meridian planes (containing the symmetry axis z) and in the equatorial plane. First, we consider the special solutions of Eq. (2.7) corresponding to the two-parametric ($K = 2$) 2D PO families in the meridian plane.^{8),9)} For these orbits, $\mu_2 = 0$ and μ_1 is in the regions

$$0 < \mu_1 < 1; \quad 1 < \mu_1 < \frac{2}{2 - \mu_1}; \quad (2.9)$$

for the hyperbolic 2D PO (with hyperbolic caustics $u = u_c$) and the elliptic 2D PO (with elliptic caustics $v = v_c$), respectively. The periodicity condition (2.7b) becomes the identity $\pi = \pi_u - \pi_v$ ($n = 1, n_u = 1$), and is fixed by

$$\pi_h = \arcsin \frac{p \frac{2}{2 - \mu_1}}{1}; \quad \pi_e = \arcsin \frac{p \frac{2}{2 - \mu_1}}{1}; \quad (2.10)$$

for the hyperbolic and elliptic 2D PO, respectively. For π , we only have the condition Eq. (2.7a). This determines μ_1 and thus I_u and I_v ($I_v = 0$ since $\mu_2 = 0$) through

$$\pi_h = \frac{p}{1}; \quad \pi_e = \frac{1}{p}; \quad (2.11)$$

for the hyperbolic and elliptic orbits, respectively.

Some examples of the hyperbolic and elliptic orbits lying along the triangular boundary side $\mu_2 = 0$ are indicated in Fig. 1; see also their geometrical illustrations in Fig. 3. The hyperbolic and elliptic tori parts are separated by the separatrix point ($\mu_1 = 1; \mu_2 = 0$) related to the long diameter (see below). Another end point of the hyperbolic tori coincides with the stationary point ($\mu_1 = \mu_2 = 0$) for the diametric

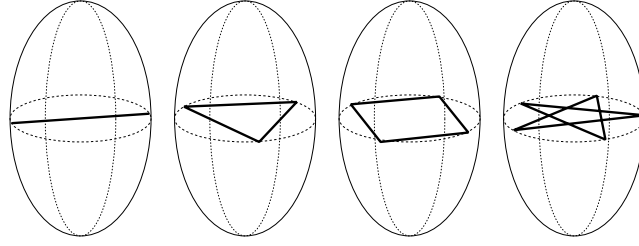


Fig. 4. Some short equatorial-plane orbits: From the left to the right, the short diameter (2;1), the triangular (3;1), the rhomboidal (4;1), and the star-shaped (5;2).

orbit in the equatorial plane. We can think of these hyperbolic and elliptic orbits as being periodic in the plane $\theta = \text{const}$ and we call them "meridian-plane periodic orbits".

For the elliptic case, the solution of Eq. (2.7) with $\theta = \theta_e(\phi)$ exists for any $n_u = 1; 2; \dots$ and $n_v = 2n_u + 1; (n_v = n_u)$ at any deformation $\mu > 1$. Examples are the triangles ($n_v = 3; n_u = 1$), the rhomboids (4;1) and the star-shaped orbits (5;2) as one-parameter families in the meridian plane. The root found from Eq. (2.7) gives the elliptic caustics with $u_c = \mu^2$ in Eq. (2.6) and the semi-axes $a_c = \frac{1}{1 - \mu^2}$ and $b_c = \mu$.

For the hyperbolic case, the solutions can be found for $n_u = 1; 2; 3; \dots$ and even n_v ($n_v \geq 2(n_u + 1)$). In Fig. 1 the "butterfly" orbit (4;2;1) is indicated as an example. The families of these orbits appear for $\mu > \mu_{\text{bif}}$ with

$$\mu_{\text{bif}} = \sin \frac{n_u}{n_v} : \quad (2.12)$$

This is the deformation where the diametric orbits $M(2;1)$ with $M = 2$ in the equatorial plane bifurcate and the hyperbolic orbits emerge from them. Their hyperbolic caustics are expressed in terms of the root of Eq. (2.7) and Eq. (2.6) with $v_c = 0$. The parameters a_c and b_c of these caustics are given by $a_c = \frac{1}{1 - \mu^2}$ and $b_c = \mu$.

2.4. Orbits in the equatorial plane

In the equatorial plane with $z = 0$, the separate families of regular polygons and diameters are the same as in a circular billiard³⁾ of radius a . The restriction $z = 0$ decreases the number K to $K = 1$. This single parameter corresponds to the angle of rotation of the polygons and the diameters about the symmetry axis z . Figure 4 illustrates the most important (shortest) equatorial-plane periodic orbits (EQPO); the diameters $M(n_v = 2; n_u = 1)$, triangles $M(3;1)$, squares $M(4;1)$ and star-shaped orbits $M(5;2)$. They satisfy, from inequalities (2.5),

$$\mu_1 = \mu_2; \quad 0 < \mu_2 < \frac{1}{2} : \quad (2.13)$$

Therefore their stationary points lie along the $\mu_2 = \mu_1$ side in the triangle, as indicated in Fig. 1.

The caustic parameters u_c and v_c for these families are defined by $u_c = 0$ and

$v_c = \operatorname{arcsinh} \left[\frac{q \cos(n' - n_v)}{1 - \sin^2(n' - n_v)} \right]$. The solutions of Eq. (2.7) for these orbits are $\mu = 0$ and $\mu = \arcsin \left(\frac{1}{1 - \sin^2(n' - n_v)} \right)^{1/2}$.

2.5. Diametric orbits along the symmetry axis

In the spheroidal cavity, there is also a diametric orbit along the z-axis (see Fig. 3). It is isolated ($K = 0$), since we have two additional restrictions $x = 0$ and $y = 0$ decreasing K by one unit more than in the previous case. The solution of Eq. (2.7) for this orbit is $\mu = 1$ and $\mu = \arcsin \left(\frac{1}{1 - \sin^2(n' - n_v)} \right)^{1/2}$. Its stationary point coincides with the separatrix values ($\mu_1 = 1$; $\mu_2 = 0$) corresponding formally to the caustic parameters ($u_c = -2$; $v_c = 0$); see the circle point with the vertical diameter in Fig. 1. (In Fig. 1b, it is very close to the stationary point for the elliptic orbits (3,1,1) in the meridian plane, which lies slightly on the right along the $\mu_2 = 0$ side.)

2.6. Bifurcations

At the deformations μ_{bif} given by Eq. (2.8), the EQPO $M(n_v; n')$ bifurcate and the 3DPO or the hyperbolic 2DPO $M(n_v; n'; n_u)$ emerge. We encounter the breaking-of-symmetry problem at these bifurcation points since the degeneracy (symmetry) parameter K changes there, for instance, from $K = 1$ of the EQPO to $K = 2$ of the 3DPO through them. Before the bifurcations ($\mu < \mu_{bif}$), the stationary points μ_1 of the 3DPO and the hyperbolic 2DPO are situated outside of the triangular tori region (2.5), and give rise to complex (μ ; μ) and complex caustics. Such formal orbits are called "complex" or "ghost" orbits.⁵⁾ They cross the $\mu_1 = \mu_2$ boundary through the stationary point of the EQPO at bifurcations ($\mu = \mu_{bif}$) and then moves into the triangular tori region for larger μ . In Fig. 1 are also indicated the stationary points for the 3DPO lying outside the physical tori region ((6,2,1) in Fig. 1a, (7,2,1) and (8,2,1) in Fig. 1b). The equatorial diameters $M(2;1)$ correspond to the limiting case, $\mu_1 = \mu_2 = 0$. They bifurcate into themselves ($K = 1$) and the hyperbolic 2DPO ($2M; M; 1$) in the meridian plane ($K = 2$) at the deformations given by Eq. (2.12).

The spherical limit is a special bifurcation point. Namely, the planar regular polygons ($K = 3$) and diameters ($K = 2$) bifurcate into the meridian 2DPO ($K = 2$), EQPO ($K = 1$) and the isolated long diameter ($K = 0$) for deformations $\mu > 1$. Another special point is the separatrix ($\mu_1 = 1$; $\mu_2 = 0$) related to the long diameter. Near this point the complicated 3DPO, elliptic and hyperbolic 2DPO having large values of $(n_u; n_v)$ and $n_u = n_v$ close to $1=2$ appear. Similar bifurcations of the 3DPO, EQPO and elliptic 2DPO appear near other boundary values of μ_1 in the triangular tori on its "creeping" side $\mu_1 = \mu_1^+ (\mu_2)$ where some kinds of 3D "creeping" orbits having large values of n_v but with finite and generally different n_u and n' appear. This is in analogy with the "creeping" singularities discussed for the elliptic orbits in the elliptic billiard²⁸⁾ near the maximum value of μ_1 , $\mu_1^{(cr)} = \cosh^2 v_b = 2 = (\mu_2^2 - 1)$, according to Eq. (A.6) at the right vertex in the "meridian-plane orbit" side $\mu_2 = 0$. The 3DPO with large number of the corners n_v and finite $n_u = n'$ approach the "creeping" elliptic orbits in the meridian plane. Another vertex corresponds to the creeping EQPO having large values of n_v and n' but for $n_v = n' \rightarrow 1=2$.

The bifurcation point related to an appearance of "creeping" orbits cannot be

reached for any finite deformation. However, even for finite deformations like superdeformed shapes, the solutions for ϵ_1 and ϵ_2 (related to the roots ϵ_1 and ϵ_2 of the periodic-orbit conditions (2.7)) can be close to the "creeping" values of ϵ_1 and ϵ_2 (related to their boundary values of (2.5)). In such cases we have to take into account such bifurcations in the trace formulas for the level density. The bifurcations of the 3D and 2D diameter-like orbits with $n_v = n_u$ close to 1=2 near the separatrix are rather long, however, so that they are not important for the shell effects discussed below.

3. Trace formulas for the prolate spheroid

3.1. Phase-space trace formula in action-angle variables

The level density $g(E)$ is obtained from the Green function $G(r; r^0; E)$ by taking the imaginary part of its trace:

$$g(E) = \sum_n \langle \delta(E - E_n) \rangle = -\frac{1}{2\pi i} \text{Im} \int_{r^0}^Z dr^0 \int_{r^0}^Z dr^0 G(r^0; r^0; E) \quad (3.1)$$

where E_n is the single-particle energy. Following Ref. 28), we apply now the Gutzwiller's trajectory expansion for the Green function $G(r; r^0; E)^{(1), (2), (10)}$. After simple transformations,²⁸⁾ we obtain the phase-space trace formula in the action-angle variables $(I; \theta)$,

$$g_{\text{scl}}(E) = \frac{1}{(2\pi)^3} \text{Re} \sum_{\text{trajectories}} \int_{I^0}^Z dI^0 \int_{I^0}^Z dI^0 \exp \left[\frac{i}{2\pi} S(I^0; I^0; t) + I^0 \theta - I^0 \theta^0 \right] \quad (3.2)$$

where the sum is taken over all classical trajectories, $I = f(I_u; I_v; I_g)$ are the actions for the spheroidal cavity, $\theta = f(\theta_u; \theta_v; \theta_g)$ the conjugate angles, and phases related with the Maslov indices.^{39), 41), (43)} The phase-space trace formula (3.2) is especially useful for integrable systems since the Hamiltonian H does not depend on the angle variables in this case, i.e., $H = H(I)$. The action

$$S(I^0; I^0; t) = \int_{I^0}^Z dI \quad (I) \quad (3.3)$$

is related to the standard definition

$$S(I^0; I^0; t) = \int_0^Z dI \quad I(\theta) \quad (3.4)$$

by the Legendre transformation

$$S(I^0; I^0; t) + I^0 \theta - I^0 \theta^0 = S(I^0; I^0; t) + I^0 \theta - I^0 \theta^0; \quad (3.5)$$

t being the time for classical motion along the trajectory. The phase will be specified below.

3.2. Stationary phase method and classical degeneracy

It should be emphasized that even for integrable systems the trace integral (3.2) is more general than the Poisson-sum trace formula which is the starting point of Refs. 5), 32), 35) for the semiclassical derivations of the level density. These two trace formulas become identical when the phase of the exponent does not depend on the angle variables. In this case, the integral over angles in (3.2) gives simply $(2\pi)^n$ where n is the dimension of the system ($n = 3$ for the spheroidal cavity), and the stationary condition for all angle variables are identities in the 2π interval. This is true for the most degenerate classical orbits like the elliptic and hyperbolic 2DPO in the meridian plane and the 3DPO with $K = n - 1 = 2$. On the other hand, for orbits with smaller degeneracy like the EQPO ($K = 1$) and the isolated long diameter ($K = 0$), the exponent phase strongly depends on angles and possesses a definite stationary point. Therefore, we have to integrate over such angles by the ISPM in the same way as for the bifurcations of the isolated diameters in the elliptic billiard.²⁸⁾

3.3. Stationary phase conditions

Due to the energy conserving δ -function, we can exactly take the integral over I_v^0 in Eq. (3.2) and result in

$$g_{\text{scl}}(\hbar) = \frac{1}{(2\pi)^3} \text{Re} \sum_{\mathbf{X}} \prod_{\mathbf{u}}^{\mathbf{Z}} d_{\mathbf{u}}^{\mathbf{Z}} \prod_{\mathbf{v}}^{\mathbf{Z}} d_{\mathbf{v}}^{\mathbf{Z}} \prod_{\mathbf{r}}^{\mathbf{Z}} d_{\mathbf{r}}^{\mathbf{Z}} dI_{\mathbf{u}}^0 dI_{\mathbf{r}}^0 \frac{1}{|J_{\mathbf{u}}^0 J_{\mathbf{r}}^0|} \exp \left[\frac{i}{\hbar} S(I_{\mathbf{u}}^0; I_{\mathbf{r}}^0; t) + I_{\mathbf{u}}^0 I_{\mathbf{r}}^0 \omega - i \frac{\pi}{2} \right] \quad (3.6)$$

The integration limits for $I_{\mathbf{u}}$ and $I_{\mathbf{r}}$ are determined by their relations to the variables (ϕ_1, ϕ_2) and by the boundaries given by Eq. (2.5). One of the trajectory ϕ_0 in the sum (3.6) is the special one which corresponds to the smooth level density g_{TF} of the Thomas-Fermi model.¹⁰⁾ For all other trajectories, we first write down the stationary phase condition for the action variables $I_{\mathbf{u}}^0$ and $I_{\mathbf{r}}^0$:

$$\frac{\partial S(I_{\mathbf{u}}^0; I_{\mathbf{r}}^0; t)}{\partial I_{\mathbf{u}}^0} = \omega_{\mathbf{u}} - \omega_{\mathbf{u}}^0 - \omega_{\mathbf{u}}^* = 2\pi M_{\mathbf{u}}; \quad (3.7a)$$

$$\frac{\partial S(I_{\mathbf{u}}^0; I_{\mathbf{r}}^0; t)}{\partial I_{\mathbf{r}}^0} = \omega_{\mathbf{r}} - \omega_{\mathbf{r}}^0 - \omega_{\mathbf{r}}^* = 2\pi M_{\mathbf{r}}; \quad (3.7b)$$

where $M = (M_{\mathbf{u}}; M_{\mathbf{v}}; M_{\mathbf{r}}) = M(n_{\mathbf{u}}; n_{\mathbf{v}}; n_{\mathbf{r}})$ and M are integer numbers which indicate the numbers of revolution along the primitive periodic orbit. The superscript asterisk means that we take the quantities at the stationary point $I_{\mathbf{u}}^0 = I_{\mathbf{u}}^*$ and $I_{\mathbf{r}}^0 = I_{\mathbf{r}}^*$. We next use the Legendre transformation (3.5). Then, the stationary phase conditions with respect to angles $(\phi_{\mathbf{u}}; \phi_{\mathbf{v}}; \phi_{\mathbf{r}})$ are given by

$$\frac{\partial S(\phi_{\mathbf{u}}^0; \omega_{\mathbf{u}}; \hbar)}{\partial \omega_{\mathbf{u}}} + \frac{\partial S(\phi_{\mathbf{r}}^0; \omega_{\mathbf{r}}; \hbar)}{\partial \omega_{\mathbf{r}}} - I_{\mathbf{u}}^0 - I_{\mathbf{r}}^0 = 0; \quad (3.8)$$

In the following derivations we have to decide whether the stationary phase conditions (all or partially) given by Eqs. (3.7) and (3.8) are identities or equations for the specific stationary points. For this purpose we have to calculate separately the contributions from the most degenerate 3DPO, the 2DPO families in the meridian plane ($K = 2$) and those from orbits with smaller degeneracy like EQPO ($K = 1$) and the isolated long diameter ($K = 0$). The latter two kinds of orbit are different from the former two kinds in the above mentioned decision concerning the integration over angles.

3.4. Three-dimensional orbits and meridian-plane orbits

The most degenerate 3DPO and the meridian-plane (elliptic and hyperbolic) 2DPO having the same values of action occupy some 3D finite areas between the corresponding caustic surfaces specified above. In this case the stationary phase conditions (3.8) for the integration over all angle variables φ_u, φ_v and φ_r are identities. The integrand does not depend on the angle variables and the result of the integration is $(2\pi)^3$. Since Eq. (3.8) is identically satisfied (the action does not depend on the angles like the Hamiltonian $H(I)$) we have the conservation of the action variables, $I_u^0 = I_u^{\infty} = I_u$ and $I_v^0 = I_v^{\infty} = I_v$, along the classical trajectory. The integrals over all φ in Eq. (3.2) yield $(2\pi)^3$ and we are left with the Poisson-sum trace formula,^{5),10)}

$$\begin{aligned} g_{\text{scl}}(\mu) &= \frac{1}{\sim^3} \text{Re} \int_{\sim^3}^X dI \left(\mu - H(I) \right) \exp \frac{2\pi i}{\sim} M \left(I - \frac{\pi}{2} M \right) \\ &= \frac{1}{\sim^3} \text{Re} \int_{\sim^3}^X dI_u dI_v \frac{1}{j^l_v j^l_u} \exp \frac{2\pi i}{\sim} M \left(I - \frac{\pi}{2} M \right) : \end{aligned} \quad (3.9)$$

It is convenient to transform the integration variables $(I_u; I_v)$ to $(\varphi_1; \varphi_2)$ defined by Eq. (2.3),

$$g_{\text{scl}}(\mu) = \frac{1}{\sim^3} \text{Re} \int_{\sim^3}^X p \int_{\sim^3}^Z \frac{d\varphi_2}{2} \frac{d\varphi_1}{2} d\varphi_1 \frac{\partial I_u}{\partial \varphi_1} \frac{1}{j^l_v j^l_u} \exp \frac{2\pi i}{\sim} M \left(I - \frac{\pi}{2} M \right) : \quad (3.10)$$

The integration limits are much simplified when written in terms of φ_i ($i = 1, 2$) and form the triangular region shown in Figs. 1. We then integrate over φ_1 expanding the exponent phase about the stationary point $\varphi_1 = \varphi_1^*$,

$$\begin{aligned} 2\pi(M - I) &= S(I; I^0; \varphi) + I^0 - I^0 \\ &= S(\mu) + \frac{1}{2} \sum_{i,j} J_{ij}(\varphi_i - \varphi_i^*)(\varphi_j - \varphi_j^*) + \dots; \end{aligned} \quad (3.11)$$

where $S(\mu)$ is the action along the periodic orbit,

$$S(\mu) = 2\pi M - n_u I_u - n_v I_v - \mu(I_u; I_v) + n_r I_r; \quad (3.12)$$

and $I_v(\prime; I_u; I_r)$ the solution of the energy conservation equation $\prime = H(I_u; I_v; I_r)$ with respect to I_v . Here the single prime index is omitted for simplicity. The J_{ij} is the Jacobian stability factor with respect to i along the energy surface,

$$J_{ij} = \frac{\partial^2 S}{\partial i \partial j} \bigg|_{i=i_i} = 2 M n_v K_{ij}; \quad (3.13)$$

and K_{ij} is the (2×2) curvature matrix of the energy surface taken at the stationary point $i = i_i$ (at the periodic orbit),

$$K_{ij} = \frac{\partial^2 I_v}{\partial i \partial j} + \frac{!_u}{!_v} \frac{\partial^2 I_u}{\partial i \partial j} + \frac{!_r}{!_v} \frac{\partial^2 I_r}{\partial i \partial j}; \quad (3.14)$$

See Appendix A for the explicit expressions of these curvatures. As we shall see below, the off-diagonal curvature K_{12} is non-zero for variables i .

Then we use the ISPM, where we keep exact finite limits for integration over i , and we finally obtain

$$g_{F_{2D}^{3D}}^{(2)}(\prime) = \frac{1}{\prime_0} \text{Re} \sum_{\alpha}^{(2)} A^{(2)} \exp(ikL) \frac{i-}{2}; \quad (3.15)$$

where $\prime_0 = \sim^2 = 2m R^2$ ($R^3 = a^2 b$ due to the volume conservation condition). The sum runs over all two-parameter families of the 3D PO or the meridian plane (elliptic and hyperbolic) 2D PO, $A^{(2)}$ is the amplitude for a 3D PO or a 2D PO,¹⁾

$$A_{F_{2D}^{3D}}^{(2)} = \frac{1}{4} \frac{L}{(M n_v R)^2} \frac{\partial I_u}{\partial i} \bigg|_{i=i_i} \frac{\text{erf } Z_1; Z_1^+ \text{ erf } Z_2; Z_2^+}{\prod_{j=2}^P \det K_j}; \quad (3.16)$$

Here, L represents "length" of the periodic orbit

$$L = \frac{2 M n_v p}{m !_v} = 2 M n_v b \sin E(\prime;) \frac{F(\prime;)}{F(\prime)} E(\prime) + \cot^p \frac{1}{1 - \sin^2}; \quad (3.17)$$

where \prime and \prime are defined by the roots of periodic-orbit equations (2.7) ($S = pL$ for cavities). This "length" taken at the stationary points i_i (the real positive roots of Eq. (2.7) through Eqs. (2.4) and (2.6)) inside the finite integration range (2.5) represents the true length of the corresponding periodic orbit. For other stationary points, the "length" is nothing else than the function (3.17) continued analytically outside the tori determined by (2.5). We introduced it formally instead of $!_v$ by the equation $!_v = 2 p M n_v = m L$ for convenience. In Eq. (3.16) we introduced also the

¹⁾ The expression (3.16) is valid also for the 2D PO ($i_2 = 0$), since the product $i_2 K_{22}$ is finite for any i_2 (see Appendix A).

generalized error function $\text{erf}(Z; Z^+)$ of the two complex arguments Z and Z^+ ,

$$\text{erf}(Z; Z^+) = \frac{2}{\pi} \int_Z^{Z^+} dz e^{-z^2} = \text{erf}(Z^+) - \text{erf}(Z); \quad (3.18)$$

with $\text{erf}(z)$ being the simple error function.⁴⁶⁾ The arguments of these error functions are given by

$$Z_1 = \frac{q}{q} \frac{i M n_v K_{11} \approx 1}{1} (2) \quad 1; \quad (3.19a)$$

$$Z_2 = \frac{i M n_v (\det K = K_{11}) \approx 2}{2} (2) \quad 2; \quad (3.19b)$$

in terms of the finite limits i given by (2.5), and taken at the stationary point $2 = 2$. We note that, for the 3D P O M (3t; t; 1) with $t = 2; 3; \dots$, the curvature K_{11} is zero at any deformation. For such orbits, one should use

$$Z_1 = \frac{q}{q} \frac{i M n_v (\det K = K_{22}) \approx 1}{1} (2) \quad 1; \quad \# \quad (3.20a)$$

$$Z_2 = \frac{i M n_v K_{22} \approx 2}{2} (2) \quad 2 + \frac{K_{12}}{K_{22}} (2) \quad 1; \quad (3.20b)$$

in place of (3.19). The latter limits (3.20) are derived by transforming the integration variable 2 to $2 (K_{12} = K_{22}) (1 \quad 1)$.

Let us consider the stationary points i far from the bifurcation points. This means that they are located far from the integration limits. Accordingly, one can transform the generalized error functions to the complex Fresnel functions with the real limits and then extend the upper limit to 1 and the lower one to -1 . In this way we obtain asymptotically the Berry-Tabor result of the standard P O T,⁵⁾ which is identical to the extended Gutzwiller's result⁹⁾ for the most degenerate (3D and meridian-plane) orbit families,

$$A_{f_{2D}^{(2)} g}^{(2)} = \frac{1}{(M n_v R)^2} \frac{L}{2 j \det K_j} \frac{\partial I_u}{\partial 1} \Big|_{i=1} : \quad (3.21)$$

The constant part of the phase in Eq. (3.15), which is independent of θ and θ , can be found by making use of the above asymptotic expression and applying the Maslov-Fedoryuk theory.^{39), 41), 43)} This theory relates the Maslov index with the number of turning and caustic points for the orbit family. For the 3D P O, the total asymptotic phase is given by

$$3D = 3D \quad \frac{1}{2} 3D + 2(M n_u - 1); \quad 3D = M (3n_v + 2n_u); \quad (3.22)$$

Here $3D$ denotes the Maslov index, the numbers of caustic and turning points traversed by the orbit. $3D$ represents the difference of the numbers of positive and negative eigenvalues of curvature K .¹⁾ For the hyperbolic and elliptic meridian

¹⁾ Since the dimension of K is 2, $3D$ is written as $3D = \text{sign}(K_1) + \text{sign}(K_2)$, where K_i is the i -th eigenvalue of K . It is also calculated by $3D = \text{sign}(K_{11}) + \text{sign}(\det K = K_{11})$ for $K_{11} \neq 0$, and $3D = \text{sign}(K_{22}) + \text{sign}(\det K = K_{22})$ for $K_{22} \neq 0$. Here, $\text{sign}(x) = 1$ for $x > 0$ and 0 for $x = 0$.

2DPO, one obtains

$$\mathcal{Z}_{2DH} = \mathcal{Z}_{2DH} + \frac{1}{2} \mathcal{Z}_{2DH} + 2(M n_u - 1); \quad \mathcal{Z}_{2DH} = 2M(n_v + n_u) \quad (3.23)$$

and

$$\mathcal{Z}_{2DE} = \mathcal{Z}_{2DE} + \frac{1}{2} \mathcal{Z}_{2DE} + 2(M n_u - 1); \quad \mathcal{Z}_{2DE} = 3M n_v \quad (3.24)$$

respectively. Note that the total phase includes the argument of the complex amplitude (3.16), and depends on both deformation and energy.

Near the bifurcation deformations, the stationary points \mathbf{z}_i are close to the boundary of the finite area (2.5). In such cases the asymptotics of the error functions are not good approximations, and we have to carry out the integration over \mathbf{z}_i in the calculation of the error functions in Eq. (3.16) exactly within the finite limits. One should also note that the contributions from "ghost" periodic orbits are important near the bifurcation points. It makes the trace formula continuous as function of deformation at all bifurcations.

When the stationary phase points \mathbf{z}_i are close to other boundaries of the tori, one has also to take the integrals with the finite limits; for instance, near the triangular side $\mathbf{z}_1 = \mathbf{z}_1^+ (\mathbf{z}_2)$ where we have the "creeping" points for the 3DPO inside the tori (2.5) and the meridian elliptic 2DPO near the end point $(\mathbf{z}_1 = \mathbf{z}_1^+, \mathbf{z}_2 = 0)$ with a large number of the vertices $n_v \gg 1$. Another sample of such special bifurcation point is the separatrix $(\mathbf{z}_1 = 1; \mathbf{z}_2 = 0)$ where 3DPO and hyperbolic 2DPO have a finite limit $n_u = n_v \gg 1 = 2$ for $n_v \gg 1$ and $n_u \gg 1$. In this case the curvature K_{11} becomes infinite and the amplitude (3.16) approaches zero. Thus, to improve the trace formula near the bifurcations, we have to evaluate the generalized error integral $\text{erf}(\mathcal{Z}_i; \mathcal{Z}_i^+)$ (or corresponding complex Fresnel functions⁴⁶⁾) in Eq. (3.16) within the finite limits \mathcal{Z}_i given by Eqs. (3.19) or (3.20).

For the spheroidal cavity we have another bifurcation at the spherical limit where the "azimuthal" Jacobian J_{22} and J_{12} (3.13) (\mathbf{z}_2 / I^2) vanishes.⁹⁾ This is the reason for the divergence of the standard POT result (3.21) in the spherical limit. Our improved trace formula (3.16) is finite in the spherical limit, because the "azimuthal" generalized error function $\text{erf}(\mathcal{Z}_2; \mathcal{Z}_2^+)$ is proportional to J_{22} in this limit and thus this "azimuthal" Jacobian is exactly canceled by that coming from the denominator of Eq. (3.16). Thus, as shown in Ref. 9), the elliptic 2DPO term ($K=2$) in the level density approach the spherical Balian-Bloch result for the most degenerate planar orbits with larger degeneracy ($K=3$),

$$\begin{aligned} q_{\text{sph}}^{(3)}(E) = & \frac{P}{kR} \int_{t=1; q \gg 2t}^{\infty} \sin \frac{2t}{q} \frac{\sin(2t-q)}{q} \\ & \sin 2kRq \sin \frac{t}{q} \frac{3}{2}q(t-1) - \frac{1}{4}; \end{aligned} \quad (3.25)$$

where $t = M n_u$ and $q = M n_v$. Note that Eq. (3.25) can be derived directly from the phase-space trace formula (3.2) or from the Poisson-sum trace formula, both rewritten in terms of the spherical action-angle variables.

3.5. Equatorial-plane orbits

We cannot apply the Poisson-sum trace formula (3.9) for equatorial-plane orbits, because, although the stationary-phase conditions for θ_v^0 and θ_u^0 in Eq. (3.8) are identities, it is not the case for the angle variable θ_u^0 . We thus apply the ISPM for the integration over θ_u^0 .

Coming back to Eq. (3.6) we transform the phase-space trace formula to new "parallel" ($\theta_v^0; I_v^0$) and "perpendicular" ($\theta_u^0; I_u^0; I_u^0$) variables as explained in Appendix B for more general (integrable and non-integrable) systems. We then make the integration over the $(I_u^0; I_u^0)$ variables in terms of the ISPM by transforming them into the θ_u^0 variables. Next, we consider the integration over the angle variable θ_u^0 by the ISPM, as there is the isolated stationary point $\theta_u^0 = 0$ or integer multiple of 2π . We expand the exponent phase in a power series of θ_u^0 about $\theta_u^0 = 0$,

$$S(I_u^0; I_v^0; \theta_u^0) = pL_{EQ} + \frac{1}{2} \sum_{ij} J_{ij}^{EQ} (\theta_u^0)^2 + \frac{1}{2} J_{??}^{EQ} (\theta_u^0)^2 + \dots; \quad (26)$$

where the stationary point $\theta_u^0 = 0$ is given by

$$\frac{L_{EQ}}{p} = \frac{a^2 \cos^2}{2} = \frac{\cos^2}{2}; \quad L_{EQ} = pa \cos \theta; \quad (3.27)$$

L_{EQ} is the length of the equatorial polygon with n_v vertices and M rotations, and is given by

$$L_{EQ} = 2M n_v R \sin \theta; \quad \theta = \theta_v = \theta_u; \quad (3.28)$$

In this way one finally obtains the amplitudes $A_{EQ}^{(1)}$ for EQPO,

$$q_{EQ}^{(1)}(\theta) = \frac{1}{n_0} \text{Re} \sum_{EQ} A_{EQ}^{(1)} \exp(i k L_{EQ} \theta); \quad (3.29)$$

$$A_{EQ}^{(1)} = \frac{\sin^3}{M n_v k R F_z^{EQ}} \text{erf } Z_1; Z_1^+ \text{erf } Z_2; Z_2^+ \text{erf } Z_3; Z_3^+; \quad (3.30)$$

see Appendix B for a detailed derivation. Here, Z_i are the limits given by Eqs. (3.19) or (3.20) for $i = 1, 2$, and $Z_3 = 0; Z_3^+ = Z_2^+$ from Eq. (B.19). The latter is related to the finite limits $\theta_u = 2\pi$ for the angle θ_u in the trace integration in Eq. (3.6), taking into account explicitly the factor 4 due to the time-reversal and spatial symmetries.

For the total asymptotic phase θ_{EQ} , one finds

$$\theta_{EQ} = \theta_{EQ} + \frac{1}{2}; \quad \theta_{EQ} = 3M n_v; \quad (3.31)$$

where θ_{EQ} is the Maslov index. We calculated this phase using the Maslov-Fedoryuk theory⁴³⁾ at a point asymptotically far from the bifurcations. Note that the total

Table I. Bifurcation points of some short periodic orbits.

periodic orbit	p_{bif}	periodic orbit	p_{bif}
(4,2,1)	2	(6,3,1)	2
(5,2,1)	1.618...	(7,3,1)	2.247...
(6,2,1)	$\frac{1}{3}$	(8,3,1)	2.414...
(7,2,1)	1.802...	(9,3,1)	2.532...
(8,2,1)	1.848...		

phase is defined as the sum of the asymptotic phase φ_{EQ} and the argument of the amplitude A_{EQ} , Eq. (3.30), so that it depends on kR and through the complex arguments of the product of the error functions. In the derivations of Eq. (3.30) we have taken into account the off-diagonal curvature as in the previous subsection, but much smaller corrections due to the mixed derivatives of the action S with respect to u and i are neglected, taking $i = i$ in Eq. (3.26).

The bifurcation points are associated with zeros of the stability factor F_z^{EQ} and given by

$$p_{\text{bif}} = \frac{\sin}{\sin(n - M)}; \quad n = 1; 2; \dots; M; \quad (3.32)$$

The bifurcation points most important for the superdeformed shell structure are listed in Table I.

When the stationary points are located inside the finite integration region far from the ends, we transform the error functions in Eq. (3.30) into the Fresnel ones and extend their arguments to ∞ , except for the case when the lower limit is exactly zero. According to the definitions of the limit, Eqs. (3.19) and (B.19), for Z_i , we have asymptotically $Z_i^+ \rightarrow +1$ ($i = 1; 2; 3$), $Z_1 = Z_3 \rightarrow 0$, $Z_2 \rightarrow 0$ for diameters and $Z_2 \rightarrow 1$ for the other EQPO. Finally, we arrive at the standard Balian-Bloch formula³⁾ for the amplitude $A_{\text{EQ}}^{(1)}$,

$$A_{\text{EQ}}^{(1)} = \frac{f_{\text{EQ}}}{kR} \frac{\sin^3}{M n_v F_z^{\text{EQ}}} \quad (3.33)$$

where $f_{\text{EQ}} = 1$ for the diameters and 2 for the other EQPO ($\text{erf}(Z_2; Z_2^+) \rightarrow f_{\text{EQ}}$ in this limit).

As seen from Eq. (3.33), there is a divergence at the bifurcation points where $F_z^{\text{EQ}} \rightarrow 0$. We emphasize that our ISPM trace formula (3.29) has no such divergences. Indeed, the stability factor F_z^{EQ} responsible for this divergence is canceled by F_z^{EQ} from the upper limit Z_3^+ , Eq. (B.19), of the last error function in Eq. (3.30), Z_3^+ / F_z^{EQ} , and we obtain the finite result at the bifurcation point:

$$A_{\text{EQ}}^{(1)} = \frac{1}{2i} \frac{\sin^2}{(2 - 1)M n_v} \text{erf}(Z_1; Z_1^+) \text{erf}(Z_2; Z_2^+) : \quad (3.34)$$

It is very important to note that there is a local enhancement of the amplitude

(3.34) by a factor of order $\frac{P}{kR} \rightarrow 1$ near the bifurcation point. This enhancement is associated with a change of the degeneracy parameter K by one unit locally near the bifurcation point and results from exactly carrying out one integration more than in the SSPM case. In general, any change of the degeneracy parameter K by ΔK is accompanied by the amplitude enhancement by $(kR)^{\Delta K=2}$ because of the ΔK extra exact integrations. These enhancement mechanism of the amplitude obtained in the ISPM is quite general and is independent of the specific choice of the potential shapes.

We mention that a more general trace formula which can be applied also to non-integrable but axially symmetric systems can be derived from the phase-space trace formula (see Appendix B).

The contribution of the equatorial diameters in Eq. (3.29) for deformations far from bifurcation points reduces to the Balian-Bloch result for the spherical diameters ($K = 2$),

$$a_{\text{sph}}^{(2)}(M) = \frac{1}{M_0} \sum_M \frac{1}{2M} \sin(4M \cdot kR): \quad (3.35)$$

The amplitude for the planar polygons in the equatorial plane vanish in the spherical limit (see Appendix B). Note that the contributions of the planar polygons in the spherical cavity, Eq. (3.25), are obtained as the limit of $A_{2D}^{(2)}$, Eq. (3.16), for elliptic orbits in the meridian plane.⁹⁾

3.6. Long diametric orbits and separatrices

As mentioned in §2, the curvatures K_{ij} become infinite near the separatrix ($\alpha_1 = 1; \alpha_2 = 0$), see Appendix C. This separatrix corresponds to the isolated long diameters ($K = 0$) along the symmetry axis. Thus, for the derivation of their contributions to the trace formula, the expansion up to the second order in action-angle variables considered above fails like for the turning and caustic points in the usual phase space coordinates. However, we can apply the Maslov-Fedoryuk theory^{39),41)-(43)} in a similar way as the calculation of the Maslov indices associated with the turning and caustic points but with the use of the action-angle variables in place of the usual phase space variables. This is similar to the derivation of the long diametric term in the elliptic billiard.²⁸⁾

Starting from the phase space trace formula (3.6) we note that the spheroidal separatrix problem differs from the one for the elliptic billiard²⁸⁾ by the integrals over the two azimuthal variables ϕ^0 and I_u^0 which are additional to the integrals over ϕ_u^0 and I_u^0 . We expand the phase of exponent in Eq. (3.6) with respect to the action I_u^0 and angle ϕ^0 about the stationary points $I_u = 0$ and an arbitrary ϕ , (for instance, $\phi = 0$), and take into account the third order terms, in a similar way as for the variables ϕ_u^0 and I_u^0 (see Appendix C). Note that we consider here small deviations from the long diameters, and ϕ , determines the azimuthal angle of the nalpoint r^0 of this trajectory near the symmetry axis.

⁹⁾ The parameter of our semiclassical expansion is in practice $\frac{P}{kL} \rightarrow \frac{P}{kR}$. It is actually large for 3D orbits ($L \sim 10R$) associated with superdeformed shell structures in nuclei.

4.2. Semiclassical shell energy

The shell energy E can be expressed in terms of the oscillating part $g_{\text{scl}}^{(1)}(\epsilon)$ of the semiclassical level density (4.1) as^{4),9),10)}

$$E = \frac{1}{t} \sum_{\epsilon} \epsilon^2 g_{\text{scl}}^{(1)}(\epsilon_F); \quad N = \sum_0^{\epsilon_F} d\epsilon g(\epsilon); \quad (4.2)$$

Here, t denotes the period for a particle moving with the Fermi energy ϵ_F along the periodic orbit ,

$$t = M T = \frac{2 M}{\omega}; \quad (4.3)$$

T being the primitive period ($M = 1$), M the number of repetitions, and ω the frequency. The Fermi energy ϵ_F is determined by the second equation of (4.2) where N is the particle number.

In the derivation of Eq. (4.2) we used an expansion of the amplitudes $A(\epsilon)$ about the Fermi energy $\epsilon = \epsilon_F$. Although $A(\epsilon)$ are oscillating functions of the energy ϵ (or kR), we can apply such an expansion, because A are much more smooth compared to the oscillations coming from the exponent function of kL . The latter oscillations are responsible for the shell structure, while the oscillations of A merely lead to slight modulations with much smaller frequencies.

Thus, the trace formula for E differs from that for g only by a factor $(\sim t)^2 = (\sim^2 k_F \sim m L)^2$ near the Fermi surface, i.e. longer orbits are additionally suppressed by a factor $1/L^2$. The semiclassical shell energy is therefore determined by short periodic orbits.

4.3. Average level density

For the purpose of presentation of the level density improved at the bifurcations we need to consider only an average level density, thus also avoiding the convergence problems that usually arise when one is interested in a full semiclassical quantization.

The average level density is obtained by folding the level density with a Gaussian of width :

$$g(\epsilon) = \frac{1}{\sqrt{2\pi}} \int_{-\infty}^{\infty} d\epsilon^0 g(\epsilon^0) e^{-\frac{(\epsilon - \epsilon^0)^2}{2\sigma^2}}; \quad (4.4)$$

The choice of the Gaussian form of the averaging function is immaterial and guided only by mathematical simplicity.

Applying now the averaging procedure defined above to the semiclassical level density (4.1), one obtains^{3),9)}

$$g_{\text{scl}}(\epsilon) = \sum_{\epsilon} g_{\text{scl}}^{(1)}(\epsilon) e^{-\frac{(\epsilon - \epsilon_F)^2}{2\sigma^2}} = \sum_{\epsilon} g_{\text{scl}}^{(1)}(\epsilon) e^{-\frac{L^2}{2R^2}}; \quad (4.5)$$

The latter equation is written specially for cavity problems in terms of the orbit length L (in units of a typical length scale R) and a dimensionless parameter ,

$$\sigma^2 = 2 \frac{P}{\omega^2}; \quad (4.6)$$

where $\bar{\alpha}$ is a dimensionless quantity for averaging with respect to kR . Thus, the averaging yields an exponential decrease of the amplitudes with increasing L and $\bar{\alpha}$. In Ref. 9), the $\bar{\alpha}$ is chosen to be 0.6. In this case, all longer orbits are strongly damped and only the short periodic orbits contribute to the oscillating part of the level density. For the study of the bifurcation phenomena in the superdeformed region, we need a significantly smaller value of $\bar{\alpha}$.

Finally, we can say that the higher the degeneracy of an orbit, the larger the volume occupied by the orbit family in the phase space, and the shorter its length, the more important is its contribution to the average density of states.

5. Quantum Spheroidal Cavity

5.1. Oscillating level density

We calculated the quantum spectrum by the spherical wave decomposition method⁵⁰⁾ in which wave functions are decomposed into the spherical waves as

$$\psi_m(r) = \sum_{l=0}^{\infty} C_{l1} j_l(kr) Y_{lm}(\theta): \quad (5.1)$$

Here, m denotes the magnetic quantum number, and $\sum_{l=0}^{\infty}$ means that l is summed over even (odd) numbers for positive (negative) parity states. j_l and Y_{lm} are the usual spherical Bessel function and spherical harmonics, respectively. The expansion coefficients C_{l1} 's are determined so that the wave function (5.1) satisfies the Dirichlet boundary condition

$$\psi_m(r = R(\theta)) = 0 \quad (5.2)$$

or equivalently,

$$\frac{d}{d\theta} Y_{lm}(\theta) \psi_m(r = R(\theta)) = 0; \quad \theta = \pi/2. \quad (5.3)$$

By inserting (5.1) into (5.3), one obtains the matrix equation

$$\sum_{l=0}^{\infty} B_{ll'}(k) C_{l1} = 0; \quad B_{ll'}(k) = \frac{d}{d\theta} Y_{lm}(\theta) j_{l'}(kR(\theta)) Y_{l'm}(\theta): \quad (5.4)$$

Truncating the summation by sufficiently large number l_c , one can obtain the energy eigenvalue $\epsilon_n = \hbar^2 k_n^2 / 2m$ by searching the roots

$$\det B(k_n) = 0: \quad (5.5)$$

Figure 5 shows the energy level diagram for the prolate spheroidal cavity as functions of axis ratio $\gamma > 1$. In Fig. 6, we plot shell structure energy

$$E(N; \gamma) = \sum_{n=1}^N \epsilon_n(\gamma) - E(N; \gamma) \quad (5.6)$$

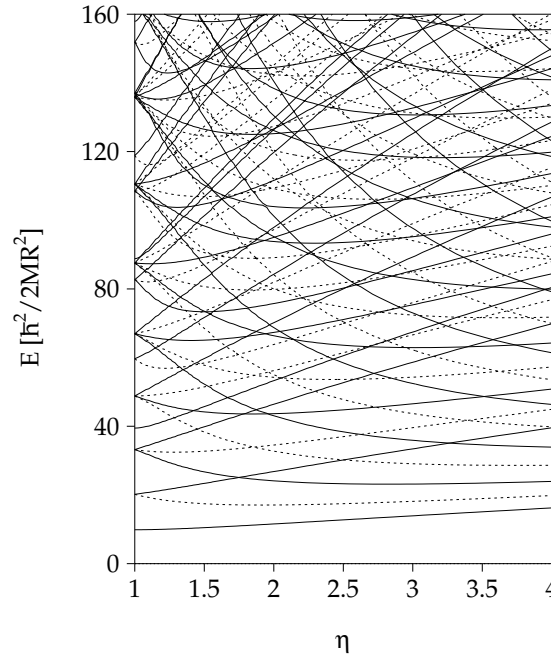


Fig. 5. Single-particle spectrum for the spheroidal cavity as a function of axis ratio η . Solid and dashed curves represent the positive and negative parity levels, respectively.

as functions of η and particle number N . As well as the strong shell effect at the spherical shape ($\eta = 1$), one clearly see a remarkable shell structure at the superdeformed shape ($\eta \approx 2$).

Next, we calculated the coarse-grained level density by the usual Strutinsky smoothing procedure by taking wave number k as smoothing variable:

$$g(k) = \frac{1}{2\pi} \int_0^{2\pi} dk^0 R f_M \left(\frac{kR - k^0 R}{\Delta} \right) g(k^0); \quad (5.7)$$

As a smoothing function $f_M(x)$, we took a Gaussian with M -th order curvature corrections

$$f_M(x) = \frac{1}{\sqrt{\pi}} e^{-x^2} L_{M-2}^{1/2}(x^2); \quad (5.8)$$

where $L_n(z)$ represents a Laguerre polynomial. Eq. (4.4) corresponds to the case of $M = 0$. In the following, we took the order of curvature corrections $M = 6$ and smoothing width $\Delta = 2.5$ with which we can nicely satisfy the plateau condition.⁴⁴⁾ The coarse-graining is also performed by the same smoothing function but with smaller Δ . We define the oscillating part of the level density by subtracting the smooth part as

$$g_{\sim}(k) = g(k) - g_{\sim}(k); \quad (5.9)$$

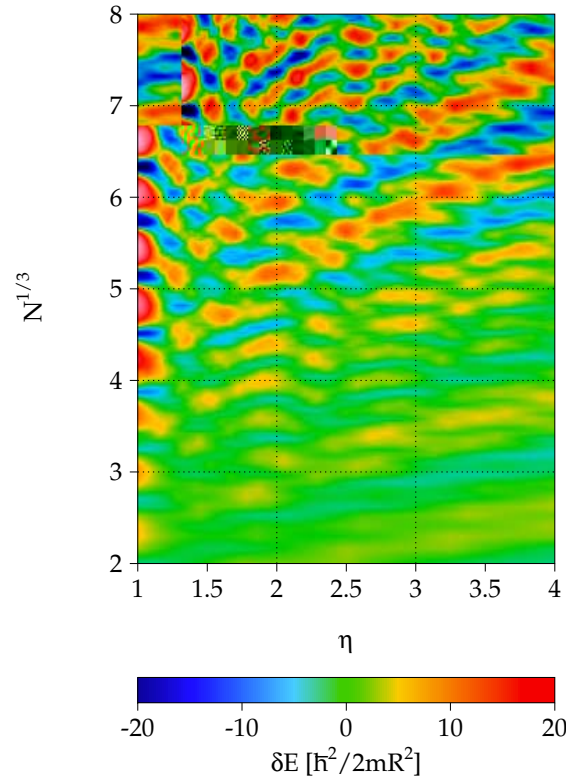


Fig. 6. Shell structure energy δE as a function of η and $N^{1/3}$, where N is the neutron (proton) number taking the spin-degeneracy factor two into account. Energies are counted in units of $\hbar^2/2mR^2$ ($\approx 30A^{-2/3}$ MeV).

The left-hand side of Fig. 7 shows $g(k)$ with $\eta = 0.3$, as functions of η and kR . One will note that a remarkable shell structure emerges at $\eta = 2$, corresponding to the superdeformed shape.

Let us consider the mechanism of this strong shell effect. If a single orbit makes a dominant contribution to the periodic-orbit sum

$$g_{cl}(\eta) = \sum_k a(k) \cos(kL) \quad (\eta = 2); \quad a(k) = A = \eta_0; \quad (5.10)$$

the major oscillating pattern in g should be determined by the phase factor of the dominant term. In that case, the positions of valley curves for g in the $(\eta; kR)$ plane are given by

$$kL = \pi = (2n + 1) \pi; \quad (n = 0; 1; 2; \dots); \quad (5.11)$$

The right-hand side of Fig. 7 shows the stationary action curves (5.11) for several periodic orbits. Green solid curves represent the triangular orbit in the meridian plane. Other longer meridian orbits also make the same behavior but with smaller distances.

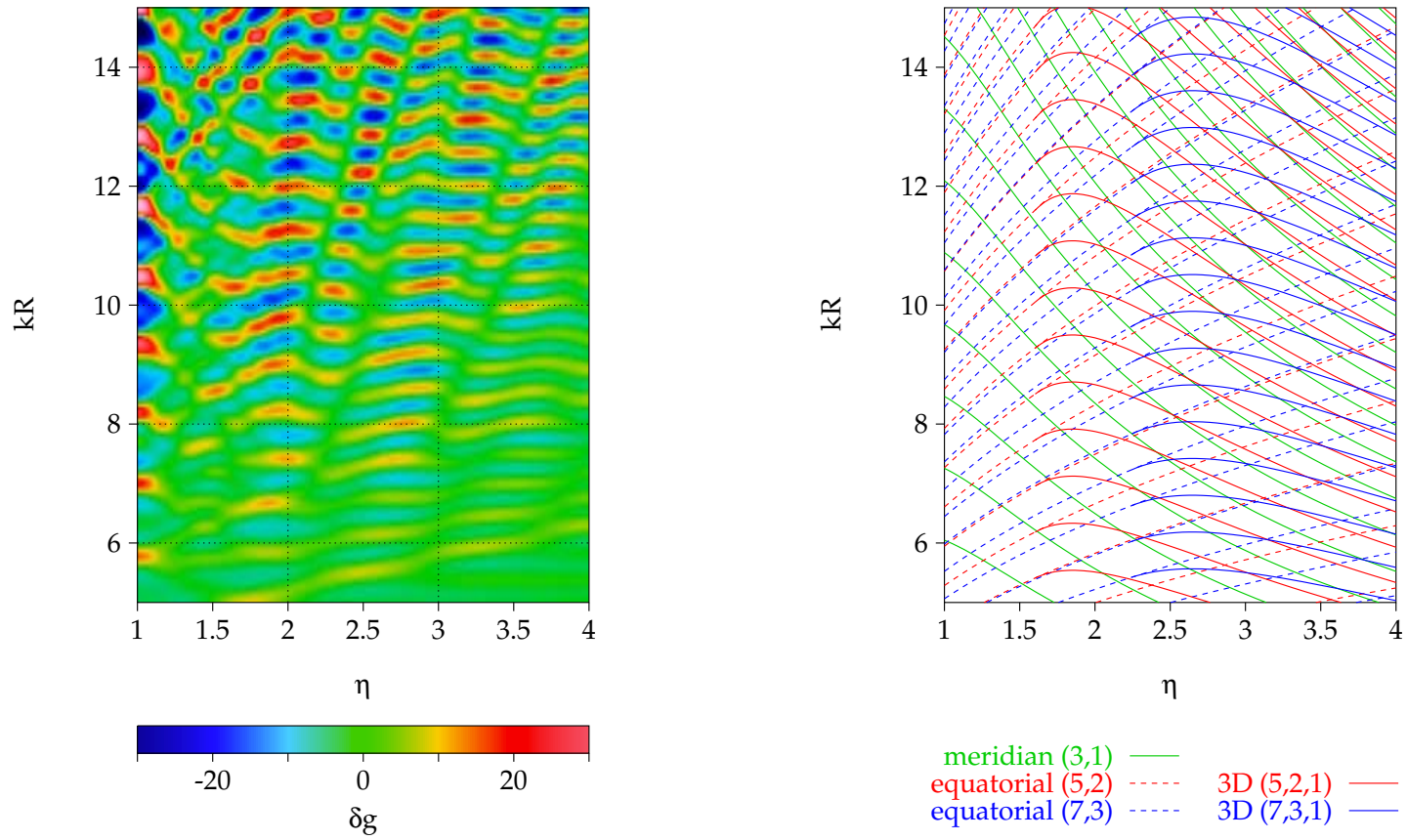


Fig. 7. Oscillating part of the single-particle level density as a function of η and kR (left-hand side) and stationary-action curves for several periodic orbits (right-hand side). Clear correspondence between the enhancement of the shell effect and the periodic-orbit bifurcations is seen.

Red dashed curves represent the star-shaped orbit with five vertices in the equatorial plane. It bifurcates at $\beta = 1.618$ and the 3D orbit (5,2,1) appears (red solid curves). The sequence (n,2,1) (n = 5;6;7;...) make the same behavior shifting the bifurcation points a little bit to larger β . Comparing with the plot of quantum g , one notices a clear correspondence between the superdeformed shell structure and the bifurcation of above star-shaped orbits. One will also note the correspondence between the bifurcations of the equatorial-plane orbits (n,3) (n = 7;8;9;...) with the hyperdeformed shell structure emerging at $\beta' \approx 2.5$. The significant shell energy gain at the superdeformed shape obtained in Fig. 6 is considered as a result of this strong shell effect in the level density.

5.2. Fourier analysis of level density

Fourier analysis is a useful tool to investigate quantum-classical correspondence in the level density.³⁾ Due to the simple form of action integral $S = \hbar kL$, one can easily Fourier transform the semiclassical level density $g_{\text{scl}}(k)$ with respect to k . Let us define the Fourier transform $F(L)$ by

$$F(L) = \int_{-\infty}^{\infty} dk e^{ikL} g(k) : \quad (5.12)$$

In actual numerical calculations, we multiply the integrand by a Gaussian truncation function as

$$F(L) = \int_{-\infty}^{\infty} dk e^{-\frac{1}{2}(k-k_0)^2} e^{ikL} g(k) : \quad (5.13)$$

Inserting the semiclassical level density (5.10), the Fourier transform is expressed as

$$F^{\text{scl}}(L) = F(L) + \frac{1}{2} \sum_n e^{i \frac{2\pi n L}{L_0}} \frac{1}{L_0} \exp \left[-\frac{1}{2} \left(\frac{L - L_0}{L_0} \right)^2 \right] : \quad (5.14)$$

This is a function which has peaks at the lengths of classical periodic orbits $L = L_0$. On the other hand, we can calculate $F(L)$ by inserting the quantum mechanical level density $g(k) = \sum_n \delta(k - k_n)$ as

$$F^{\text{qm}}(L) = \sum_n \frac{1}{2} e^{-\frac{1}{2}(k_n - k_0)^2} e^{ik_n L} : \quad (5.15)$$

It should present successive peaks at orbit lengths $L = L_0$. Thus we can extract information on classical periodic orbits from the quantum spectrum. In the left-hand side of Fig. 8, we plot the Fourier transform (5.15) as a function of L and β . In the right-hand side of Fig. 8, lengths of classical periodic orbits L_0 are shown. Red curves represent the orbits $M(n_v; 2; 1)$ ($n_v = 4; 5; 6; \dots$). We found strong Fourier peaks at $\beta' \approx 2$ corresponding to the periodic orbits (5,2,1), (6,2,1) and (7,2,1) just after the bifurcation points. We also found Fourier peaks at $\beta' \approx 2.5$ corresponding to the periodic orbits (7,3,1) and (8,3,1) etc. Thus, we can conclude that those periodic orbit bifurcations play essential roles in the emergence of superdeformed and hyperdeformed shell structures.

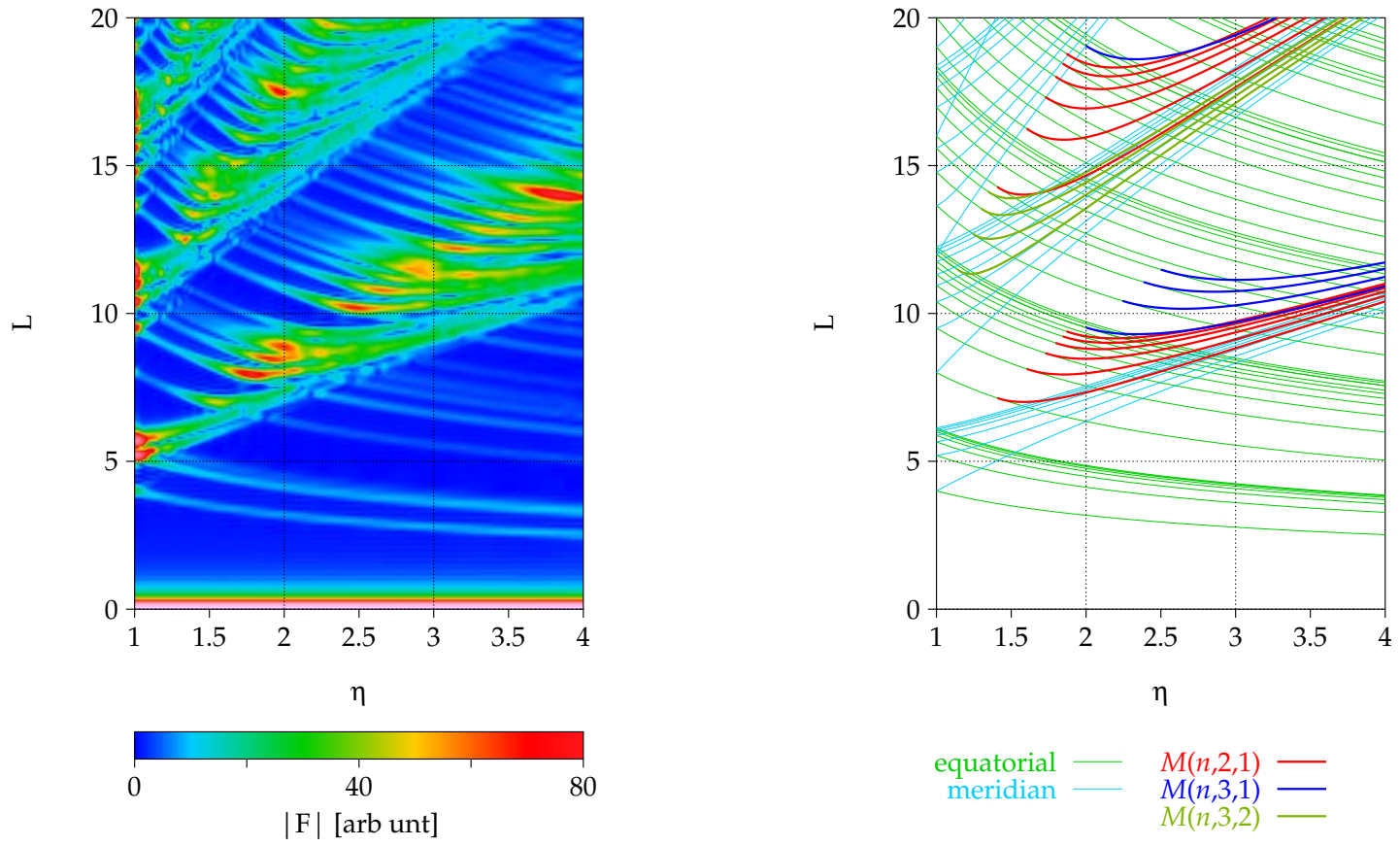


Fig. 8. Fourier amplitude $|F(L)|$ of the single-particle level density (left-hand side) and lengths of classical periodic orbits (right-hand side).

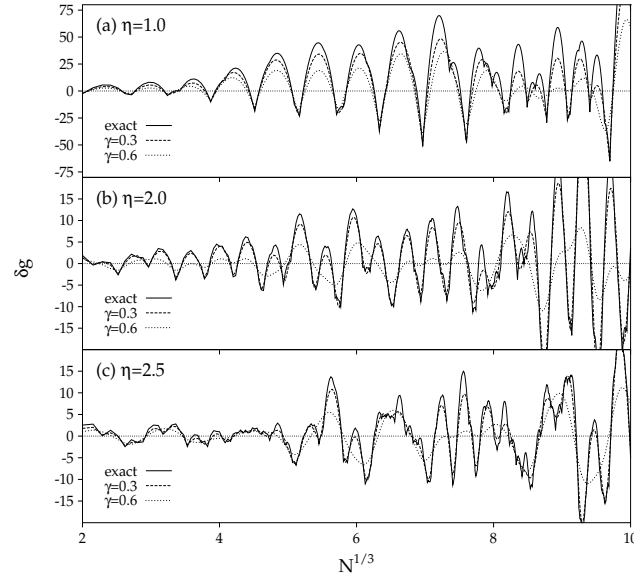


Fig. 9. Shell structure energies plotted as functions of $N^{1/3}$. Solid curves represent the exact shell structure energies. Dashed and dotted curves represent those calculated by using the coarse-grained level density $g(k)$ with the smoothing width $\gamma = 0.3$ and 0.6 , respectively.

5.3. Coarse-grained shell structure energy

In order to prove that the shell structure at the superdeformed shape is due to the bifurcated orbits, we calculated the 'coarse-grained' shell energy defined by

$$E_{\sim}(N) = \int_{K_F(\sim)}^{\infty} \epsilon(k) g(k) dk - \int_{K_F(\sim)}^{\infty} \epsilon(k) g_{\sim}(k) dk; \quad (5.16)$$

where the smoothed Fermi wave number K_F in each term is determined so that they satisfy the particle number condition

$$\int_{K_F(\sim)}^{\infty} g(k) dk = \int_{K_F(\sim)}^{\infty} g_{\sim}(k) dk = N; \quad (5.17)$$

By coarse-graining with width γ , a shell structure of resolution $kR = \gamma$ is extracted. Classical orbits relevant for such a structure are those with lengths

$$L < L_{\max} = \frac{2}{\gamma} R; \quad (5.18)$$

Taking $\gamma = 0.6$, contributions from periodic orbits with $L > 10R$ are smeared out. Around the superdeformed shape, bifurcated orbits have lengths $L \sim 10R$ and those contributions are significantly weakened by smoothing with $\gamma = 0.6$, and the major oscillating pattern of E should disappear if those bifurcated orbits are responsible for the superdeformed shell effect. In Fig. 9, the coarse-grained shell energies (5.16) calculated for $\eta = 1; 2; 3$, with $\gamma = 0.3$ and 0.6 , are compared with the exact shell

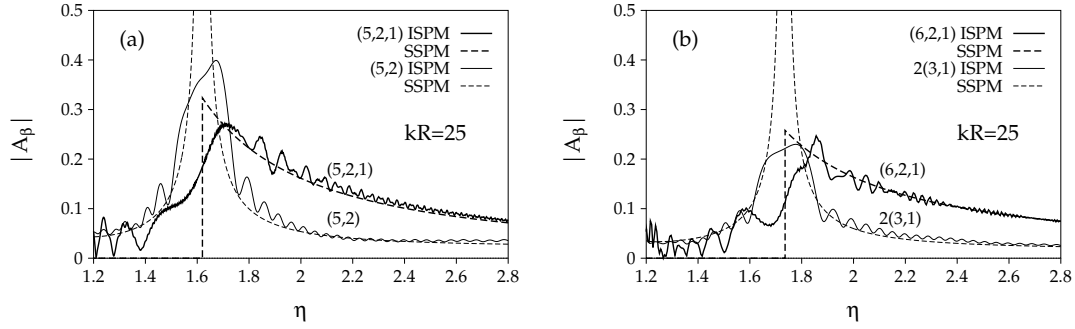


Fig. 10. (a) Semiclassical amplitudes \mathcal{A}_{3D} for the 3DPO (5,2,1) and \mathcal{A}_{EQ} for the EQPO (5,2), calculated at $kR = 25$ by the ISPM, are plotted as functions of the deformation parameter by thick and thin solid curves, respectively. They are compared with the SSPM amplitudes (dashed curves). (b) The same as (a) but for the 3DPO (6,2,1) and the EQPO 2(3,1).

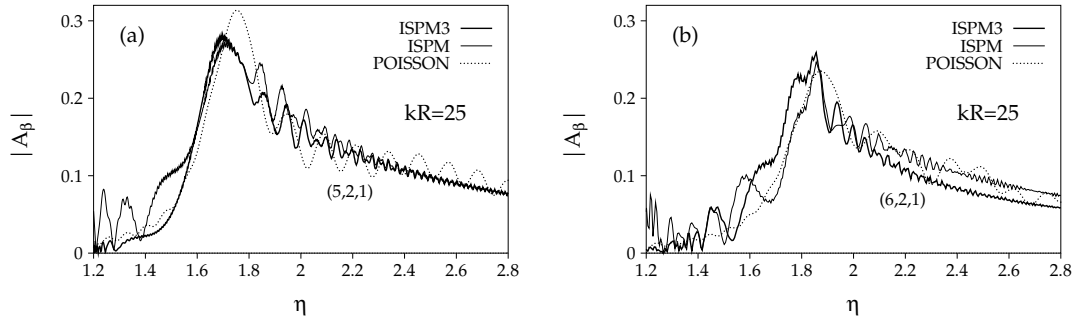


Fig. 11. (a) ISPM3 amplitudes for the 3DPO (5,2,1), calculated at $kR = 25$, are shown as function of deformation by thick-solid curves. For comparison, the ISPM amplitudes and the results of exact integration in the Poisson-sum trace formula are plotted with thin-solid and thick-dotted curves, respectively. (b) The same as (a) but for the 3DPO (6,2,1).

structure energies. In the upper panel, one observes that the spherical shell structure survives after smoothing with $\gamma = 0.6$, indicating that the major structure is determined by orbits whose lengths are sufficiently shorter than $10R$. On the other hand, in the middle panel, one notices that the major oscillating pattern of the superdeformed shell structure is considerably broken after smoothing with $\gamma = 0.6$. The same argument is valid also for $\gamma = 3$. This strongly supports the significance of bifurcated orbits for the superdeformed and hyperdeformed shell structures.

x6. Enhancement of semiclassical amplitudes near the bifurcation points

In this section, we present some results of the semiclassical ISPM calculation, which clearly show enhancement phenomena of the semiclassical amplitudes \mathcal{A}_{3D} and \mathcal{A}_{EQ} near the bifurcation points.

Figure 10a shows the modulus of the complex amplitude A_{3D} (Eq. (3.16)) for the 3DPO (5;2;1) and A_{EQ} (Eq. (3.30)) for the EQPO (5;2) as functions of the deformation parameter η . They are compared with those of the SSPM. The SSPM

amplitude for the EQPO (5;2) is divergent at the bifurcation deformation $\beta_{\text{bif}} = 1.618:::$, while the ISPM amplitude is finite and continuous through this bifurcation point with a rather sharp maximum at this point. This is due to a local change of the symmetry parameter K from 1 to 2 at the bifurcation, and the associated enhancement of the amplitude is of the order \sqrt{kR} . As seen from Fig. 10a, the ISPM amplitude for the (5;2;1) is continuous through the bifurcation point and exhibit a remarkable enhancement a little on the right of it. It approaches the SSPM amplitude given by Eq. (3.21) away from the bifurcation point. The ISPM enhancement for the 3DPO is also of the order \sqrt{kR} , because of the same change of the degeneracy parameter K from 1 to 2 as in the case of the bifurcating EQPO. The same is true for the 3DPO (6,2,1) and the EQPO 2(3,1) as shown in Fig. 10b.

In Fig. 11, we consider corrections from the 3rd-order terms in the expansion of the action about the stationary point. Here we incorporate the 3rd-order terms in the ϕ_1 variable (ISPM 3) which are expected to be important for the 3DPO (6,2,1) whose curvature K_{11} is identically zero (see Appendix D). We also show results of exact integration in the Poisson-sum trace formula (3.10) (marked POISSON). One sees that the results of the ISPM 3 for the (5;2;1) and (6;2;1) orbits are in good agreement with those of the ISPM in the most important regions near the bifurcations and on the right-hand sides of them. It is gratifying to see that the ISPM and the ISPM 3 amplitudes \tilde{A}_{3Dj} for (5;2;1) and (6;2;1) are also in good agreement with the results of exact integration in the Poisson-sum trace formula. With the 3rd-order corrections, excessive ghost orbit contributions in the ISPM (bumps in the ISPM amplitudes in the left-hand side of the bifurcation point) are removed and better agreement with the result of exact integration is obtained. Except for that, the corrections due to the 3rd-order terms are rather small, and good convergence is achieved up to the second-order terms.

The amplitudes \tilde{A}_j are slightly oscillating functions of kR . Since the period of this oscillation is much larger than that of the shell energy oscillation, one can use the expansion about the Fermi energy ϵ_F (or $k_F R$) in the derivations of both the semiclassical ISPM shell energy E_{sc1} and the oscillating level density g_{sc1} (3.15). Figure 12 shows the semiclassical amplitudes A_{3D} for the 3DPO (5,2,1) and A_{EQ} for the EQPO (5;2) as functions of kR at $\beta = 1.618:::$ (top panel) and $\beta = 2$ (bottom panel). In this figure, the semiclassical amplitudes A_{3D} for the 3DPO (6,2,1) and A_{EQ} for the EQPO 2(3,1) are also plotted as functions of kR at the bifurcation point $\beta = \sqrt{3}$ (middle panel). We see that for $\beta = 2$ the amplitudes \tilde{A}_{3Dj} for the 3DPO (5;2;1) and (6;2;1) become much larger than the amplitude \tilde{A}_{EQj} for the EQPO.

x7. Comparison between quantum and semiclassical calculations

In this section we present results of calculation of level densities and shell energies with the use of the quantum Strutinsky method and the semiclassical ISPM, and make comparisons between the quantum and semiclassical calculations. In the quantum calculations, the averaging parameter $\sigma = 0.3$ is used.

Figure 13 shows oscillating level densities g for relatively small deformations; QM and ISPM denote the g obtained by the quantum Strutinsky method and the

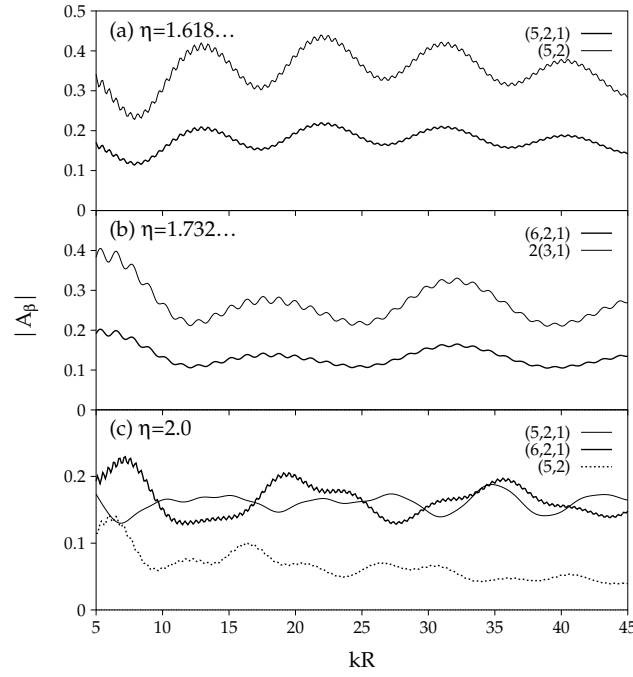


Fig. 12. (a) Semiclassical amplitudes \mathcal{A}_{3D} for the 3DPO $(5,2,1)$ and \mathcal{A}_{EQ} for the EQPO $(5,2)$ are plotted by bold and thin solid curves, respectively, as functions of kR at the bifurcation point $\eta = 1.618\dots$. (b) The same as (a) but for the 3DPO $(6,2,1)$ and the EQPO $2(3,1)$ at the bifurcation point $\eta = 1.732\dots$. (c) Semiclassical amplitudes \mathcal{A}_{3D} for $(5,2,1)$, $(6,2,1)$ and \mathcal{A}_{EQ} for $(5,2)$ are plotted by thin-solid, thick-solid and dotted curves, respectively, as functions of kR at $\eta = 2.0$.

semiclassical ISPM, respectively. For $\eta = 1.2$ we obtain a good convergence of the periodic orbit sum (4.1) by taking into account the short elliptic 2DPO with $n_v = 12$, $n_u = 1$, the short EQPO with the maximum vertex number $p_{max} = M(n_v)_{max} = 14$, and the maximum winding number $t_{max} = M(n_v) = 1$ ($M = 1; n_v = 1$). The ISPM result is in good agreement with the quantum result. For the bifurcation point $\eta = \sqrt{2}$ of the butterfly orbit $(4;2;1)$ and $\eta = 1.5$ slightly on the right of it, the convergence of the periodic-orbit sum is attained by taking into account the contributions from the bifurcating orbits, $(4;2;1)$ and the twice-repeated diameter $2(2;1)$ with $t_{max} = 2$, in addition to the 2DPO and the EQPO considered in the $\eta = 1.2$ case.

Figure 14 presents the oscillating level densities for the bifurcation deformations; $\eta = 1.618\dots$ for the EQPO $(5;2)$, $\eta = \sqrt{3}$ for the EQPO $2(3;1)$, and $\eta = 2$ for the triply repeated equatorial diameters $3(2;1)$. It is interesting to compare this figure with Fig. 15 where some results of simplified semiclassical calculations are shown. In the top panel of Fig. 15, the SSPM is used instead of the ISPM. We see that the SSPM is a good approximation for $\eta = 1.2$. In the middle and bottom panels, only bifurcating orbits are taken into account in the periodic-orbit sum: only the 3DPO $(5;2;1)$, the EQPO $(5;2)$ and the butterfly $(4;2;1)$ are accounted for in the middle

panel, while only the 3DPO (5;2;1), (6;2;1), (7;2;1), (8;2;1) in the bottom panel. By comparing with the corresponding ISPM results shown in Fig. 15, we see that, for $\eta = 1.618 \dots$ and 2, the major patterns of the oscillation are determined by these short 3DPO.

Figures 16 and 17 show the shell energies which respectively correspond to the oscillating level densities shown in Figs. 13 and 14. Again, we see good agreement between the results of the semiclassical ISPM and the quantum calculations. For $\eta = 1.2$, a good convergence is attained by including only the shortest elliptic 2DPO and EQPO, in the same way as for the level density ρ , see Ref. 9). For $\eta = \sqrt{2}$ and 1.5, properties of the ISPM shell energies are similar to those considered for the elliptic billiard in Ref. 28). Now, let us more closely examine the bifurcation effects in the superdeformed region by comparing Fig. 17 with Fig. 18. In the top panel of Fig. 18, we show the ISPM result for $\eta = 1.618 \dots$ in which only the bifurcating 3DPO (5;2;1), the short EQPO (5;2) and the hyperbolic 2DPO (4;2;1) are taken into account. In the middle panel of this figure, we show the ISPM shell energies at $\eta = 1.732 \dots$, calculated by taking into account only the 3DPO (5;2;1), the bifurcating 3DPO (6;2;1) and the EQPO (2;3;1). These comparisons clearly indicate that a few dominant periodic orbits determine the property of quantum shell structure at those bifurcation deformations. The bottom panel in this figure shows the dominating contributions of only a few shortest 3DPO at $\eta = 2.0$. Evidently, the short 3DPO (5;2;1), (6;2;1), (7;2;1) and (8;2;1) determine the major oscillating pattern of the shell energy. Thus, we can say that they are responsible for the formation of the shell structure at large deformations around the superdeformed

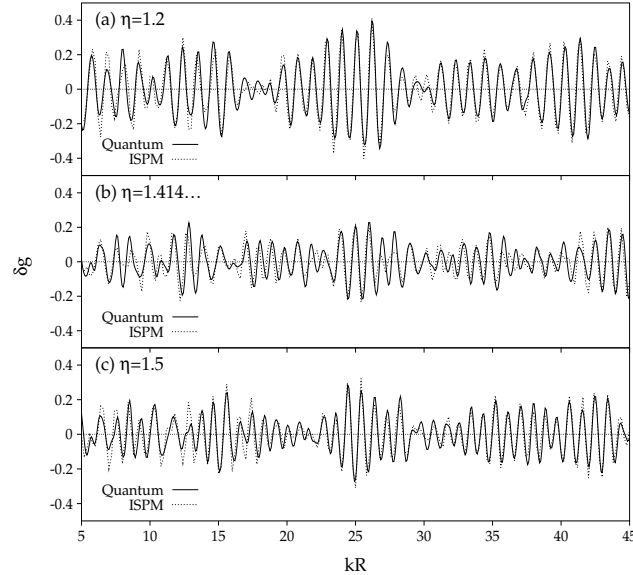


Fig. 13. Oscillating level densities evaluated by the semiclassical ISPM, and by the quantum mechanics are shown by dotted and solid curves, respectively, as functions of kR for several deformations.

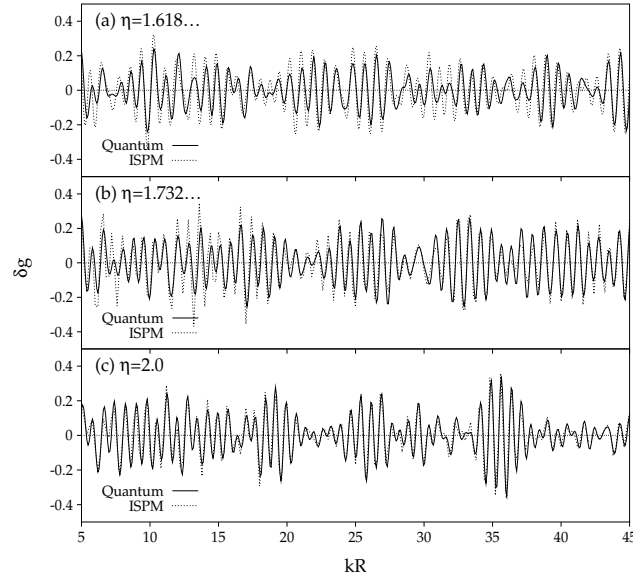


Fig. 14. The same as Fig. 13 but for larger deformations.

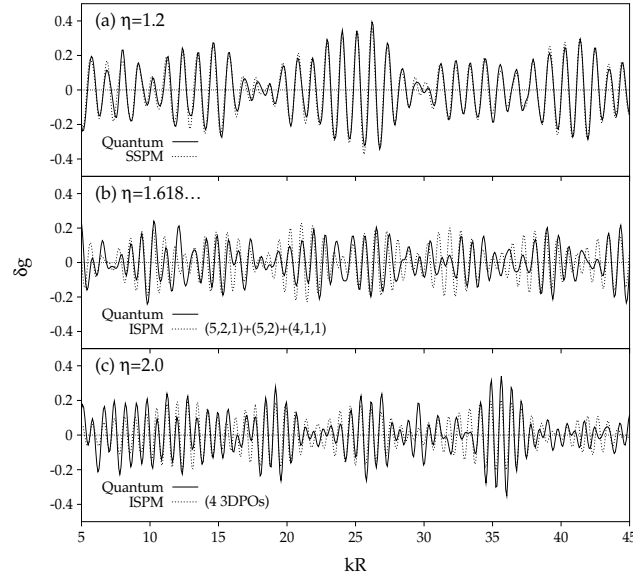


Fig. 15. Comparison of the oscillating level densities calculated by quantum mechanics (solid curves) and those obtained by some specific semiclassical calculations (dotted curves); (a) the top panel shows a comparison with the SSPM result for $\eta = 1.2$, (b) the middle panel shows the ISPM result in which only the bifurcating 3DPO $(5;2;1)$, the EQPO $(5;2)$, and the 2DPO butterfly $(4;2;1)$ are taken into account for the POT sum in Eq. (3.15) for $\eta = 1.618\dots$, (c) the bottom panel shows the ISPM result in which only the four shortest 3DPO are taken into account for $\eta = 2.0$.

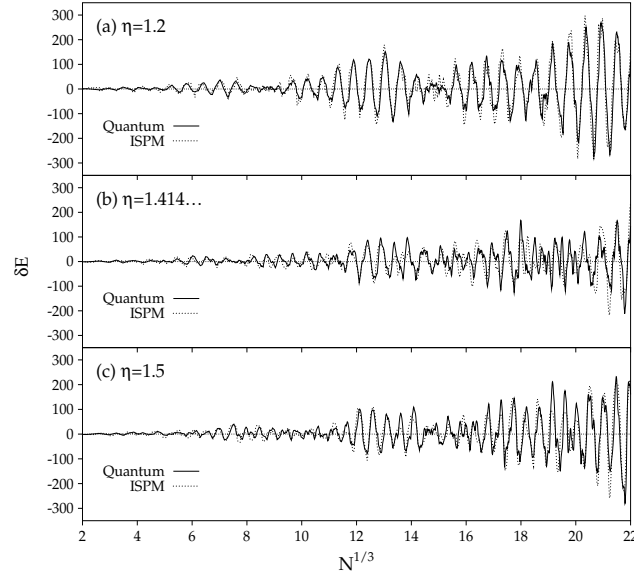


Fig. 16. Sem iclassical ISPM and quantum shell energies (in unit of ϵ_0) are plotted by dotted and solid curves, respectively, as functions of $N^{1/3}$.

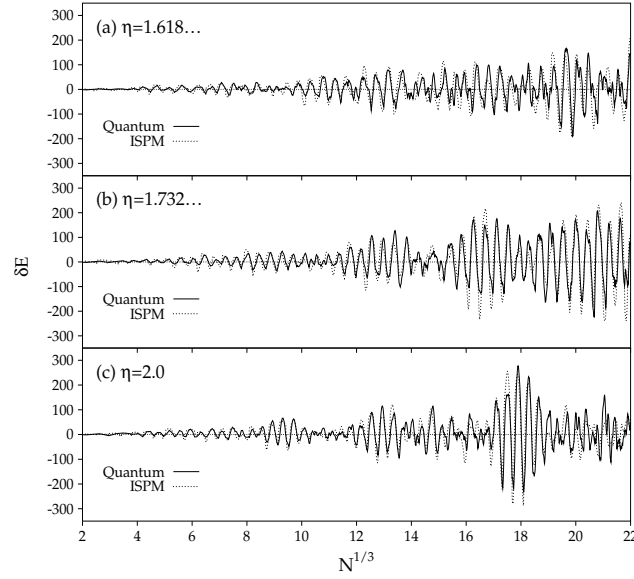


Fig. 17. The same as Fig. 16 but for larger deformations.

shape. These results of calculation are in good agreement with those obtained in Ref. 23) from the analysis of the length spectra (Fourier transforms of the quantum level densities).

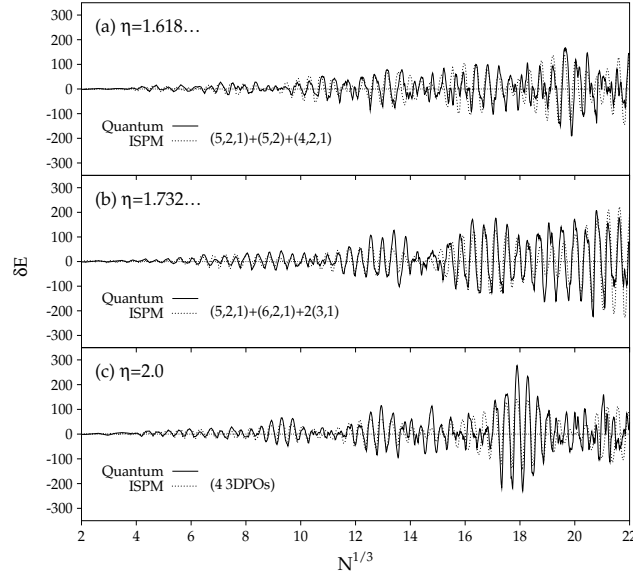


Fig. 18. Comparison of quantum shell energies (solid curves) with those obtained with specific semiclassical calculations (dotted curves): (a) the top panel shows the ISPM result for $\eta = 1.618...$, where only the bifurcating orbits $(5,2,1)$, $(5,2)$ and $(4,2,1)$ are taken into account, (b) the middle panel shows for $\eta = 1.732...$ the contributions of only the three orbits; the 3DPO $(5,2,1)$ and $(6,2,1)$, and the EQPO $2(3,1)$, (c) the bottom panel shows for $\eta = 2.0$ the contributions of only the four shortest 3DPO to the ISPM sum.

8. Conclusion

We have obtained an analytical trace formula for the 3D spheroidal cavity model, which is continuous through all critical deformations where bifurcations of periodic orbits occur. We find an enhancement of the amplitudes A_j at deformations $1.6(2.0)$ due to bifurcations of 3D orbits from the short 2D orbits in the equatorial plane. The reason of this enhancement is quite general and independent of the specific potential shapes. We believe that this is an important mechanism which contributes to the stability of superdeformed systems, also in the formation of the second minimum related to the isomeric states in nuclear fission. Our semiclassical analysis may therefore lead to a deeper understanding of shell structure effects in superdeformed fermionic systems (not only in nuclei or metal clusters but also, e.g., in deformed semiconductor quantum dots whose conductance and magnetic susceptibilities are significantly modified by shell effects).

Acknowledgements

A.G.M. gratefully acknowledges the financial support provided under the COE Professorship Program by the Ministry of Education, Science, Sports and Culture of Japan (Monbu-sho), giving him the opportunity to work at the RCNP, and thanks Prof. H. Toki for his warm hospitality and fruitful discussions. We acknowledge valu-

able discussions with Prof. M.B rack. Two of us (A.G.M. and S.N.F.) thank also the Regensburger Universitätsstiftung Hans Vielberth and Deutsche Forschungsgemeinschaft (DFG) for the financial support.

References

- 1) M.C.Gutzwiller, J.Math.Phys. 12 (1971), 343; and earlier references quoted therein.
- 2) M.C.Gutzwiller, Chaos in Classical and Quantum Mechanics, (Springer-Verlag, New York, 1990).
- 3) R.B.Balian and C.Bloch, Ann.of Phys. 69 (1972), 76.
- 4) V.M.Stutinsky, Nukleonika 20 (1975), 679;
V.M.Stutinsky and A.G.M agner, Sov.Phys.Part.Nucl. 7 (1977), 138.
- 5) M.V.Berry and M.Tabor, Proc.Roy.Soc.Lond.A 349 (1976), 101.
- 6) M.V.Berry and M.Tabor, J.of Phys.A 10 (1977), 371.
- 7) S.C.Creagh and R.G.Littlejohn, Phys.Rev.A 44 (1990), 836; J.of Phys.A 25 (1992), 1643.
- 8) V.M.Stutinsky, A.G.M agner, S.R.O fengenden and T.D ssing, Z.Phys.A 283 (1977), 269.
- 9) A.G.M agner, S.N.Fedotkin, F.A.Ivanyuk, P.Meier, M.B rack, S.M.Reim ann and H.Koizumi, Ann.of Phys. 6 (1997), 555;
A.G.M agner, S.N.Fedotkin, F.A.Ivanyuk, P.Meier and M.B rack, Czech.J.Phys. 48 (1998), 845.
- 10) M.B rack and R.K.Bhaduri, Sem iclassical Physics (Addison-W esley, 1997).
- 11) H.Frisk, Nucl.Phys.A 511 (1990), 309.
- 12) K.A rita and K.M atsuyanagi, Nucl.Phys.A 592 (1995), 9.
- 13) M.B rack, S.M.Reim ann and M.Sieber, Phys.Rev.Lett. 79 (1997), 1817; M.B rack, P.Meier, S.M.Reim ann, and M.Sieber, in: Similarities and Differences between Atomic Nuclei and Clusters, eds.Y.Abe et al., (AIP, New York, 1998), p.17.
- 14) H.Nishioka, K.Hansen and B.R.M ottelson, Phys.Rev.B 42 (1990), 9377.
- 15) M.B rack, S.Creagh, P.Meier, S.Reim ann, and M.Seidl, in: Large Cluster of Atoms and Molecules, eds.T.P.M artin, (Kluwer, Dordrecht 1996), p.1;
M.B rack, J.Blaschke, S.C.Creagh, A.G.M agner, P.Meier and S.M.Reim ann, Z.Phys.D 40 (1997), 276.
- 16) S.Frauendorf, V.M.Kolomoietz, A.G.M agner and A.I.Sanzhur, Phys.Rev.B 58 (1998), 5622.
- 17) S.M.Reim ann, M.Persson, P.E.Lindelof, and M.B rack, Z.Phys.B 101 (1996), 377.
- 18) J.M a and K.Nakamura, Phys.Rev.B 60 (1999), 10676 and 11611.
- 19) J.Blaschke and M.B rack, Europhys.Lett. 50 (2000), 294.
- 20) J.M a and K.Nakamura, Phys.Rev.B 62 (2000), 13552.
- 21) J.M a and K.Nakamura, preprint archive cond-mat/0108276 (2001), submitted to Phys.Rev.Lett.
- 22) A.Sugita, K.A rita and K.M atsuyanagi, Prog.Theor.Phys. 100 (1998), 597.
- 23) K.A rita, A.Sugita and K.M atsuyanagi, Prog.Theor.Phys. 100 (1998), 1223.
- 24) A.G.M agner, S.N.Fedotkin, K.A rita, K.M atsuyanagi and M.B rack, Phys.Rev.E 63 (2001), 065201(R).
- 25) H.Nishioka, M.Ohta and S.Okai, Mem.Konan Univ.Sci.Ser. 38 (2) (1991), 1 (unpublished).
- 26) H.Nishioka, N.Nitanda, M.Ohta and S.Okai, Mem.Konan Univ.Sci.Ser. 39 (2) (1992), 67 (unpublished).
- 27) K.A rita, A.Sugita and K.M atsuyanagi, Proc.Int.Conf.on "Atomic Nuclei and Metallic Clusters", Prague, 1997, Czech.J.of Phys. 48 (1998), 821.
- 28) A.G.M agner, S.N.Fedotkin, K.A rita, K.M atsuyanagi, T.M isu, T.Schachner and M.B rack, Prog.Theor.Phys. 102 (1999), 551.
- 29) S.C.Creagh, Ann.of Phys. 248 (1997), 60.
- 30) S.Tomovic, M.Grinberg and D.Ullmo, Phys.Rev.Lett. 75 (1995), 4346;
D.Ullmo, M.Grinberg and S.Tomovic, Phys.Rev.E 54 (1996), 136.
- 31) M.Sieber, J.of Phys.A 30 (1997), 4563.
- 32) P.J.Richens, J.of Phys.A 15 (1982), 2110.

- 33) P. Meier, M. Brack and C. Creagh, Z. Phys. D 41 (1997), 281.
- 34) H. Waaalkens, J. Wiersig and H. R. Dullin, Ann. of Phys. 260 (1997), 50.
- 35) M. Sieber, J. of Phys. A 29 (1996), 4715.
- 36) H. Schomerus and M. Sieber, J. of Phys. A 30 (1997), 4537;
M. Sieber and H. Schomerus, J. of Phys. A 31 (1998), 165.
- 37) M. Brack, P. Meier, and K. Tanaka, J. of Phys. A 32 (1999), 331.
- 38) C. Chester, B. Friedman, F. Ursell, Proc. Cambridge Philos. Soc. 53 (1957), 599.
- 39) M. V. Fedoryuk, Sov. J. of Comp. Math. and Math. Phys. 4 (1964), 671; 10 (1970), 286.
- 40) A. D. Bruno, preprint Inst. Prikl. Mat. Akad. Nauk SSSR Moskva (1970), 44 (in Russian).
- 41) V. P. Maslov, Theor. Math. Phys. 2 (1970), 30.
- 42) M. V. Fedoryuk, Saddle-point method (Nauka, Moscow, 1977, in Russian).
- 43) M. V. Fedoryuk, Asymptotics: Integrals and sums (Nauka, Moscow, 1987, in Russian).
- 44) V. M. Stutinsky, Nucl. Phys. A 122 (1968), 1; and earlier references quoted therein.
- 45) M. Brack et al., Rev. Mod. Phys. 44 (1972), 320.
- 46) M. Abramowitz and I. A. Stegun, Handbook of mathematical functions (Overpublications INC., New York, 1964).
- 47) Paul F. Byrd and Morris D. Friedman, Handbook of Elliptic Integrals for Engineers and Scientists, (Springer-Verlag, 1971).
- 48) L. D. Landau and E. M. Lifshits, Theoretical Physics, Vol. 1, Classical mechanics (Nauka, Moscow, 1973, in Russian).
- 49) I. S. Gradshteyn and I. M. Ryzhik, Tables of integrals, series, and products, 6th ed., (Academic Press, 2000).
- 50) T. Mukhopadhyay and S. Pal, Nucl. Phys. A 592 (1995), 291.

Appendix A

— Curvatures —

A.1. Three-dimensional orbits

The action is written as

$$S = 2M(n_v I_v + n_u I_u + n_r I_r); \quad (\text{A } \cdot 1)$$

where I_u , I_v and I_r are the partial actions. In a dimensionless form,

$$I_u = \frac{p}{2} \tilde{I}_u; \quad I_v = \frac{p}{2} \tilde{I}_v; \quad I_r = \frac{p}{2} \tilde{I}_r; \quad (\text{A } \cdot 2)$$

where

$$\tilde{I}_u = 2 \int_{z_0}^{z_+} \frac{dz}{1 - z^2} \sqrt{\frac{q}{(z^2 - z_-^2)(z^2 - z_+^2)}}; \quad (\text{A } \cdot 3a)$$

$$\tilde{I}_v = 2 \int_{z_+}^{z_0} \frac{dz}{z^2 - 1} \sqrt{\frac{q}{(z^2 - z_-^2)(z^2 - z_+^2)}}; \quad (\text{A } \cdot 3b)$$

$$\tilde{I}_r = \frac{p}{2}; \quad (\text{A } \cdot 3c)$$

z_{\pm} are related to the α_i variables by

$$z_+^2 + z_-^2 = \alpha_1 + 1; \quad z_+^2 z_-^2 = \alpha_1 \alpha_2; \quad (\text{A } \cdot 4)$$

In terms of the elliptic integrals, (A · 3) can be expressed as

$$\tilde{I}_u = \frac{2}{z_+} (z_+^2 - 1) F(k) - \alpha_2 (z_-^2; k) + z_+^2 E(k); \quad (\text{A } \cdot 5a)$$

$$\tilde{I}_v = \frac{1}{z_+} (z_+^2 - z_-^2) [F(\alpha'; k) - (\alpha'; n; k)] - z_+^2 E(\alpha'; k) + z_0 \sin \alpha'; \quad (\text{A } \cdot 5b)$$

with

$$k = \frac{z}{z_+}; \quad n = \frac{1}{1} \frac{z^2}{z_+^2}; \quad \nu = \arcsin \sqrt{\frac{z_b^2 - z_+^2}{z_b^2 - z^2}};$$

$$z_b = \cosh v_b = \frac{e^{\frac{v_b}{2}} + e^{-\frac{v_b}{2}}}{2}; \quad (\text{A } \cdot 6)$$

Here, we used the standard definitions of the elliptic integrals of the first and the third kind¹⁾

$$F(\nu; k) = \int_0^{\nu} \frac{dx}{\sqrt{1 - k^2 \sin^2 x}}; \quad (\text{A } \cdot 7a)$$

$$E(\nu; k) = \int_0^{\nu} \sqrt{1 - k^2 \sin^2 x} dx; \quad (\text{A } \cdot 7b)$$

$$\nu(n; k) = \int_0^{\nu} \frac{dx}{(1 - n \sin^2 x) \sqrt{1 - k^2 \sin^2 x}}; \quad (\text{A } \cdot 7c)$$

and on it argument $\nu = \pi/2$ for complete elliptic integrals. The action (A.1) is written as

$$S = 2\pi M \left(n_v \mathcal{I}_v + n_u \mathcal{I}_u + n_r \mathcal{I}_r \right); \quad (\text{A } \cdot 8)$$

The curvatures K_{ij} of the energy surface $\mathcal{H} = H(\nu_1; \nu_2; \nu)$ are defined as

$$K_{ij} = \frac{1}{2} K_{ij} = \frac{\partial^2 \mathcal{I}_v}{\partial \nu_i \partial \nu_j} + \frac{\mathcal{I}_u}{\mathcal{I}_v} \frac{\partial^2 \mathcal{I}_u}{\partial \nu_i \partial \nu_j} + \frac{\mathcal{I}_r}{\mathcal{I}_v} \frac{\partial^2 \mathcal{I}_r}{\partial \nu_i \partial \nu_j}; \quad (\text{A } \cdot 9)$$

and the frequency ratios in Eq. (A.9) are given by

$$\frac{\mathcal{I}_u}{\mathcal{I}_v} = \frac{\partial \mathcal{I}_v}{\partial \mathcal{I}_u} = \frac{\partial \mathcal{I}_v / \partial \nu_1}{\partial \mathcal{I}_u / \partial \nu_1}; \quad (\text{A } \cdot 10)$$

$$\frac{\mathcal{I}_r}{\mathcal{I}_v} = \frac{\partial \mathcal{I}_v}{\partial \mathcal{I}_r} = \frac{2\nu_2}{\partial \mathcal{I}_v / \partial \nu_2} + \frac{\mathcal{I}_u}{\mathcal{I}_v} \frac{\partial \mathcal{I}_u}{\partial \nu_2}; \quad (\text{A } \cdot 11)$$

We used here the properties of Jacobians for the transformations from the variables $(\mathcal{I}_u, \mathcal{I}_r)$ to $(\nu_1; \nu_2)$. For the first derivatives of the actions (A.3) with respect to ν_1 and ν_2 , one obtains

$$\frac{\partial \mathcal{I}_u}{\partial \nu_1} = \frac{1}{z_+} F(k); \quad \frac{\partial \mathcal{I}_v}{\partial \nu_1} = \frac{1}{2z_+} F(\nu; k); \quad (\text{A } \cdot 12a)$$

¹⁾ The definitions of elliptic integrals (A.7) are related with those in Ref. 46) as $F(\nu; k) = F(\nu; k)$ and $\nu(n; k) = \nu(n; k) - \nu(\sin \alpha)$.

$$\frac{\partial \mathcal{I}_u}{\partial z_2} = \frac{1}{z_+} (z^2; k); \quad \frac{\partial \mathcal{I}_v}{\partial z_2} = C_F F'(\cdot; k) + C(\cdot; n; k); \quad (\text{A } 12b)$$

with

$$C_F = \frac{z_+^2}{2z_+} \frac{1}{z_2} = \frac{1}{2z_+ (z^2 - 1)}; \\ C = \frac{z_+^2}{2z_+} \frac{z^2}{z_2} = \frac{z_+^2}{2z_+ (z_+^2 - 1) (z^2 - 1)}; \quad (\text{A } 13)$$

For the second derivatives of these actions, one obtains

$$\frac{\partial^2 \mathcal{I}_u}{\partial z_1^2} = \frac{1}{2z_+^3} \frac{1}{k^2} (k^2; k) - F(k) - \frac{\partial z^2}{\partial z_1} k^2 \frac{\partial z_+^2}{\partial z_1} - \frac{\partial z_+^2}{\partial z_1} F(k); \quad (\text{A } 14a)$$

$$\frac{\partial^2 \mathcal{I}_v}{\partial z_1^2} = \frac{1}{4z_+^3} \frac{1}{k^2} (F'; k^2; k) - F'(F'; k) - \frac{\partial z^2}{\partial z_1} k^2 \frac{\partial z_+^2}{\partial z_1} \\ - \frac{\partial z_+^2}{\partial z_1} F'(F'; k) + \frac{2z_+^2}{\partial z_1} \frac{\partial F'}{\partial z_1}; \quad (\text{A } 14b)$$

$$\frac{\partial^2 \mathcal{I}_u}{\partial z_2^2} = \frac{1}{2z_+^5 k_1^2} (z^2; k) + 2z_+^2 \frac{\partial (z^2; k)}{\partial n} + \frac{1+k^2}{k} \frac{\partial (z^2; k)}{\partial k}; \quad (\text{A } 14c)$$

$$\frac{\partial^2 \mathcal{I}_v}{\partial z_2^2} = \frac{\partial C_F}{\partial z_2} F'(F'; k) + C_F \frac{1}{\partial z_2} \frac{\partial F'}{\partial z_2} + \frac{\partial F'(F'; k)}{\partial k} \frac{\partial k}{\partial z_2} + \frac{\partial C}{\partial z_2} (F'; n; k) \\ + C \frac{\partial (F'; n; k)}{\partial F'} \frac{\partial F'}{\partial z_2} + \frac{\partial (F'; n; k)}{\partial n} \frac{\partial n}{\partial z_2} + \frac{\partial (F'; n; k)}{\partial k} \frac{\partial k}{\partial z_2}; \quad (\text{A } 14d)$$

and

$$\frac{\partial^2 \mathcal{I}_u}{\partial z_1 \partial z_2} = \frac{1}{2z_+^5 k_1^2} F(k) + \frac{1+k^2}{k} \frac{\partial F(k)}{\partial k}; \quad (\text{A } 14e)$$

$$\frac{\partial^2 \mathcal{I}_v}{\partial z_1 \partial z_2} = \frac{1}{4z_+^5 k_1^2} F'(F'; k) - \frac{(1+1-2z_b^2) \tan}{\partial z_b^2 k_1} + \frac{1+k^2}{k} \frac{\partial F'(F'; k)}{\partial k}; \quad (\text{A } 14f)$$

Here,

$$x = \arcsin \frac{z_+}{z_b}; \quad k_1 = \frac{1}{\sqrt{1-k^2}}; \quad = \arcsin \frac{z_+}{z_b}; \quad (\text{A } 15)$$

and

$$\frac{\partial z^2}{\partial z_1} = \frac{1}{2} \frac{1}{1 - \frac{1}{(1-1)^2 + 4}} = \frac{1}{2} \frac{1}{1 - \frac{z_+^2 + z^2}{z_+^2 - z^2}}; \quad (\text{A } 16)$$

$$\frac{\partial'}{\partial_1} = \frac{1}{2} \frac{\frac{\partial z^2}{\partial_1} (z_b^2 - z_+^2) - \frac{\partial z_+^2}{\partial_1} (z_b^2 - z_+^2)}{(z_b^2 - z_+^2) (z_b^2 - z_+^2) (z_+^2 - z^2)}; \quad (\text{A } \cdot 17)$$

$$\frac{\partial k^2}{\partial_2} = \frac{1 + k^2}{z_+^4 k_1^2}; \quad (\text{A } \cdot 18)$$

$$\begin{aligned} \frac{\partial C_F}{\partial_2} &= \frac{z^2 - 2z_+^2 - 1}{4z_+^3 (1 - z_+^2)^2 (z_+^2 - z^2)}; \\ \frac{\partial C}{\partial_2} &= \frac{2(3z_+^2 + z^2) - 2z_+^2 (z_+^2 - z^2)^2}{4z_+^3 \frac{2}{2} (z_+^2 - z^2)}; \end{aligned} \quad (\text{A } \cdot 19)$$

$$\frac{\partial'}{\partial_2} = \frac{2z_b^2 - (1 + 1) \tan}{2z_b^2 z_+^4 k_1^3 - 2}; \quad (\text{A } \cdot 20)$$

$$\frac{\partial n}{\partial_2} = \frac{1}{(1 - z_+^2)^2 (z_+^2 - z^2)}; \quad (\text{A } \cdot 21)$$

$$\frac{\partial z^2}{\partial_2} = \frac{1}{z_+^2 - z^2}; \quad (\text{A } \cdot 22)$$

Derivatives of elliptic integrals are given by

$$\frac{\partial F(' ; k)}{\partial k} = \frac{1}{k} ((' ; k^2 ; k) - F(' ; k)); \quad (\text{A } \cdot 23)$$

$$\frac{\partial (' ; n ; k)}{\partial'} = \frac{1}{(1 - n \sin^2 ')}; \quad (\text{A } \cdot 24)$$

$$\frac{\partial (' ; n ; k)}{\partial n} = \frac{1}{n} [_{21} (' ; n ; k) - (' ; n ; k)]; \quad (\text{A } \cdot 25)$$

$$\frac{\partial (' ; n ; k)}{\partial k} = \frac{1}{k} [_{13} (' ; n ; k) - (' ; n ; k)]; \quad (\text{A } \cdot 26)$$

with

$$_{ij} (' ; n ; k) = \int_0^Z \frac{dx}{(1 - n \sin^2 x)^i (1 - k^2 \sin^2 x)^{j-2}}; \quad (\text{A } \cdot 27)$$

A.2. Meridian-plane orbits

For the meridian-plane orbits for which $L_z = 0$ ($\alpha_2 = 0$), the actions I_u and I_v defined by Eq. (2.3) can be simplified. In the dimensionless form (A.2) one obtains for the elliptic orbits

$$I_u = 2 \int_0^{\pi} \sqrt{1 - E - \frac{1}{2} \sin^2 \theta} d\theta; \quad (\text{A.28a})$$

$$I_v = \int_0^{\pi} \sqrt{1 - E - \frac{1}{2} \sin^2 \theta} d\theta + \frac{1}{2} \int_0^{\pi} \frac{1}{\sqrt{1 - E - \frac{1}{2} \sin^2 \theta}} d\theta \quad (\text{A.28b})$$

Here we used the identity⁴⁷⁾

$$\int_0^{\pi} \frac{1}{\sqrt{1 - k^2 \sin^2 \theta}} d\theta = \frac{2}{1 - k^2} \int_0^{\pi} \sqrt{1 - k^2 \sin^2 \theta} d\theta = (1 - k^2) \int_0^{\pi} \sqrt{1 - k^2 \sin^2 \theta} d\theta \quad (\text{A.29})$$

In this subsection, we omit the suffix "1" for the variable θ for shortness. For the hyperbolic orbits,

$$I_u = 2 \int_0^{\pi} \sqrt{1 - E - \frac{1}{2} \sinh^2 \theta} d\theta; \quad (\text{A.30a})$$

$$I_v = \int_0^{\pi} \sqrt{1 - E - \frac{1}{2} \sinh^2 \theta} d\theta + \frac{1}{2} \int_0^{\pi} \frac{1}{\sqrt{1 - E - \frac{1}{2} \sinh^2 \theta}} d\theta \quad (\text{A.30b})$$

Equations (A.28) and (A.30) may be regarded as parametric equations in terms of the parameter θ for the energy surface of the meridian-plane orbits, $(I_u, I_v, L_z = 0)$, for its elliptic and hyperbolic parts, respectively.

The curvature K_{11} of the energy curve for the meridian-plane orbits can be obtained by differentiating Eqs. (A.28) and (A.30) implicitly through the parameter θ . In this way one obtains Eq. (3.13) with the dimensionless derivatives for the elliptic orbits

$$\frac{\partial I_u}{\partial \theta} = \frac{1}{2} \sqrt{1 - E - \frac{1}{2} \sin^2 \theta}; \quad (\text{A.31a})$$

$$\frac{\partial^2 I_u}{\partial \theta^2} = -\frac{1}{2} \frac{1}{\sqrt{1 - E - \frac{1}{2} \sin^2 \theta}}; \quad (\text{A.31b})$$

$$\frac{\partial I_v}{\partial \theta} = \frac{1}{2} \sqrt{1 - E - \frac{1}{2} \sinh^2 \theta} + \frac{1}{2} \frac{1}{\sqrt{1 - E - \frac{1}{2} \sinh^2 \theta}}; \quad (\text{A.31c})$$

$$\frac{\partial^2 I_v}{\partial \theta^2} = -\frac{1}{4} \frac{1}{\sqrt{1 - E - \frac{1}{2} \sinh^2 \theta}} - \frac{1}{2} \frac{1}{\sqrt{1 - E - \frac{1}{2} \sinh^2 \theta}} + \frac{1}{2} \frac{1}{\sqrt{1 - E - \frac{1}{2} \sinh^2 \theta}}; \quad (\text{A.31d})$$

For the hyperbolic orbits,

$$\frac{\partial \mathcal{I}_u}{\partial} = F(\mathcal{P}^-); \quad (\text{A } 32a)$$

$$\frac{\partial^2 \mathcal{I}_u}{\partial^2} = \frac{1}{2} \left(\mathcal{P}^- \right) F(\mathcal{P}^-); \quad (\text{A } 32b)$$

$$\frac{\partial \mathcal{I}_v}{\partial} = \frac{1}{2} F(\mathcal{H}; \mathcal{P}^-) F(\mathcal{P}^-); \quad (\text{A } 32c)$$

$$\frac{\partial^2 \mathcal{I}_v}{\partial^2} = \frac{1}{4} \left(\mathcal{H}; \mathcal{P}^- \right) \left(\mathcal{P}^- \right) z + F(\mathcal{P}^-) F(\mathcal{H}; \mathcal{P}^-); \quad (\text{A } 32d)$$

Thus, for elliptic orbits

$$\mathcal{K}_{11} = \frac{1}{4} \frac{F(\mathcal{E}; \mathcal{P}^-)}{F(\mathcal{P}^-)} \left(\mathcal{P}^- \right) \left(\mathcal{E}; \mathcal{P}^- \right) + \frac{\mathcal{P}^- \frac{1}{2} \left(\mathcal{P}^- \right)}{\mathcal{P}^- \frac{1}{2} \left(\mathcal{P}^- \right)}; \quad (\text{A } 33)$$

and for hyperbolic orbits

$$\mathcal{K}_{11} = \frac{1}{4} \frac{F(\mathcal{H}; \mathcal{P}^-)}{F(\mathcal{P}^-)} \left(\mathcal{P}^- \right) \left(\mathcal{H}; \mathcal{P}^- \right); \quad (\text{A } 34)$$

A.3. Equatorial plane orbits

For the equatorial limit $\mathcal{P}^- = 1$ one obtains from (A.4)

$$z^2 = 0; \quad z_+^2 = 1; \quad (\text{A } 35)$$

We thus obtain in this limit ($\mathcal{K} \rightarrow 0$)

$$\begin{aligned} \frac{\partial \mathcal{I}_u}{\partial} &= \frac{\mathcal{P}^-}{2\mathcal{P}^- + 1}; & \frac{\partial \mathcal{I}_v}{\partial} &= \frac{\mathcal{P}^- \mathcal{E}_Q}{2\mathcal{P}^- + 1}; \\ \frac{\partial z^2}{\partial} &= \frac{1}{1 + 1} = \frac{1}{2}; \end{aligned} \quad (\text{A } 36)$$

and

$$\begin{aligned} \frac{\partial^2 \mathcal{I}_u}{\partial^2} &= \frac{(1 - \mathcal{P}^-)}{8(1 + 1)^{5/2}}; \\ \frac{\partial^2 \mathcal{I}_v}{\partial^2} &= \frac{1}{8(1 + 1)^{5/2}} \left((2 - 1) \mathcal{E}_Q + \frac{1}{2} \sin(2 \mathcal{E}_Q) \right) \\ &\quad - \frac{\mathcal{P}^- \frac{1}{2} \left(\mathcal{P}^- \right)}{z_b^2 \frac{1}{2} \left(\mathcal{P}^- \right)}; \\ \mathcal{E}_Q &= \arcsin \frac{z_b^2}{z_b} \end{aligned} \quad (\text{A } 37)$$

Substituting (A.36) and (A.37) into (A.9) one finally obtains the equatorial limit

$$K_{11}^{EQ} = \frac{z_b^2(2 - 1) + (+ 1)}{8z_b^2(+ 1)^2 - z_b^2(+ 1)}; \quad (A.38a)$$

In the same way, one obtains

$$K_{22}^{EQ} = \frac{z_b^2(2 -) + (+ 1)}{8z_b^2(+ 1)^2 - z_b^2(+ 1)}; \quad (A.38b)$$

$$K_{12}^{EQ} = \frac{3z_b^2(+ 1)}{8z_b^2(+ 1)^2 - z_b^2(+ 1)}; \quad (A.38c)$$

The determinant of the curvature matrix for EQPO becomes

$$\det K^{EQ} = \frac{1}{32z_b^2(+ 1)^2} \quad (A.39)$$

which is negative for any orbit and for any deformation > 1 . It shows that bifurcations of EQPO's occur only through the zeros of stability factor F_z^{EQ} .

Appendix B

—— Derivation of trace formula for the equatorial-plane orbits ——

We start with the phase-space trace formula^{(9),(28),(31),(40)}

$$\begin{aligned} g_{cl}(\") = \text{Re} \sum_{\alpha} \frac{dq^{\alpha} dp^0}{(2\pi)^3} \exp \left[-i \int_0^{\alpha} H(q^0; p^0) dt + p^0 p^0 q^0 - \frac{i}{2} \right]; \quad (B.1) \end{aligned}$$

where the sum runs over all trajectories, $q = q(t; q^0; p^0)$ determined by the fixed initial momentum p^0 and the initial coordinate q^0 , $H(q; p)$ is the classical Hamiltonian, α the phase related to the Maslov index, number of caustics and turning points.^{(39),(41),(43)} The $S(p^0; p^0; t)$ is the action in the mixed phase-space representation,

$$S(p^0; p^0; t) = \int_{p^0}^{p^0} dp \, q(p); \quad (B2)$$

related to the standard definition of the action $S(q^0; q^0; \")$,

$$S(q^0; q^0; \") = \int_{q^0}^{q^0} dq \, p(q) \quad (B3)$$

by the Legendre transformations (the integration by parts),

$$S(p^0; p^0; t) = S(q^0; q^0; \") + p^0 p^0 q^0; \quad (B.4)$$

being the time formation of the particle along the trajectory. The $J(p_z^0; p_z^0)$ in Eq. (B.1) is the Jacobian for the transformation from p_z^0 to p_z^0 . Here, we introduced the local system of the phase-space coordinates $q = q_k; q_z$ and $p = p_k; p_z$ splitting the vectors into the parallel and perpendicular components with respect to the trajectory.

For the equatorial-plane periodic orbits (EQPO) one of the perpendicular components q_z and p_z can be taken along the symmetry axis z , say z and p_z , keeping for other perpendicular components the same x, q_z and p_z . After the transformation to this local phase-space coordinate system and integration over the "parallel" momentum $p_k = p = \frac{p}{2m}$ by using the δ -function in Eq. (B.1), one obtains for the contribution from the EQPO ($K = 1$)

$$q_{EQ}^{(1)}(\omega) = \frac{1}{(2\pi)^3} \text{Re} \int^X \int^Z \frac{dq_k^0}{j_k^0} \frac{dq_z^0}{j_z^0} \frac{dp_z^0}{j_z^0} J(p^0; p^0)^{-1/2} \exp \left[\frac{i}{\hbar} S(p^0; p^0; t) + \frac{i}{2} \right]; \quad (B.5)$$

where $q_k = \partial H / \partial p_k = p/m$ is the velocity. In the spheroidal action-angle variables, $q_k = v, p_k = I_v, q_z = I_z, p_z = I_z, z = I_u, p_z = I_u$, and we have

$$q_{EQ}^{(1)}(\omega) = \frac{1}{(2\pi)^3} \text{Re} \int^X \int^Z \frac{dI_v^0}{j_v^0} \frac{dI_z^0}{j_z^0} \frac{dI_u^0}{j_u^0} J(I^0; I^0)^{-1/2} \exp \left[\frac{i}{\hbar} S(I^0; I^0; t) + \frac{i}{2} \right]; \quad (B.6)$$

We now perform the integrations using the expansion of the action S about the stationary points

$$S(I^0; I^0; t) + \frac{i}{2} = S^{(0)} + \frac{1}{2} \sum_{ij} J_{ij} (I_i - I_i^0) (I_j - I_j^0) + \frac{1}{2} J_z (I_z - I_z^0)^2 + \dots \quad (B.7)$$

Here we omit the corrections associated with mixed derivatives of type $\partial^2 S / \partial I_u \partial I_z$ for simplicity. J_z is the Jacobian corresponding to the second variation of the action S with respect to the angle variable I_u ,

$$J_z^{EQ} = \frac{\partial^2 S}{\partial I_u^2} + 2 \frac{\partial^2 S}{\partial I_u \partial I_z} + \frac{\partial^2 S}{\partial I_z^2} = \frac{\partial I_u^0}{\partial I_u} \left(2 \frac{\partial I_u^0}{\partial I_u} + \frac{\partial I_u^0}{\partial I_z} \right) : \quad (B.8)$$

This quantity can be expressed in terms of the curvatures K^{EQ} and the Gutzwiler's stability factor F_z^{EQ} ,

$$F_z^{EQ} = \frac{\partial I_u^0}{\partial I_u} \left(2 \frac{\partial I_u^0}{\partial I_u} + \frac{\partial I_u^0}{\partial I_z} \right) \cdot \frac{\partial I_u^0}{\partial I_z} = 4 \sin^2 \frac{1}{2} M n_v \arccos 1 - 2 \sin^2 \frac{1}{2} ; \quad (B.9)$$

as

$$J_{\varphi}^{EQ} = \frac{F_z^{EQ}}{(J_u - J_u^2, =J,)^{EQ}} = \frac{F_z^{EQ}}{2 M n_v (K_u - K_u^2, =K,)^{EQ}} \quad (B \cdot 10)$$

In these equations we used simple identical Jacobian transformations

$$\frac{\partial I_u^0}{\partial I_u^0} = \frac{\partial (I_u^0; I^0)}{\partial (I_u^0; I^0)} = \frac{\partial I_u^0}{\partial I_u^0} \frac{\partial I^0}{\partial I^0} = J_u - J_u, \frac{J_u'}{J},$$

The curvature K_u^{EQ} is the quantity K_u defined in (B.13), evaluated at stationary point $\varphi_1 = \varphi_2 = \varphi$ given by Eq. (3.27), and so on.

The integrand of (B.6) does not depend on the angles (φ_v, φ') and we obtain simply $(2\pi)^2$ for the integration over these angle variables. We transform integration variables $(I_u; I')$ into $(\varphi_1; \varphi_2)$ to obtain simple integration limits, and integrate over $(\varphi_1; \varphi_2)$ by the ISPM. In this way we obtain

$$g_{EQ}^{(1)}(\varphi) = \frac{r}{2\pi^3} \text{Re} \int_{-\infty}^{\infty} e^{i(kL)} = 2) \frac{1}{!_v} \frac{\partial (I_u; I')}{\partial (\varphi_1; \varphi_2)} \frac{1}{J_{\varphi} \text{jdet} J^{EQ}} \text{erf}(Z_{\varphi}; Z_{\varphi}^+; Z_1; Z_1^+; Z_2; Z_2^+) \quad (B \cdot 11)$$

where

$$\text{erf}(x; x^+; y; y^+; z; z^+) = \frac{2}{\pi} \int_{-\infty}^{\infty} \int_{-\infty}^{\infty} \int_{-\infty}^{\infty} dx_y dy_z dz e^{-x^2 - y^2 - z^2}; \quad (B \cdot 12)$$

Note that the integration limits for the internal integrals over y and z in $\text{erf}(x; x^+; y; y^+; z; z^+)$ in general depend on the variable of the next integrations, $y = y(x)$ and $z = z(x; y)$. Here we define curvatures in the $(I_u; I')$ variables as

$$J_u = \frac{\partial^2 S}{\partial I_u^2} = 2 M n_v K_u; \quad J' = \frac{\partial^2 S}{\partial I'^2} = 2 M n_v K';$$

$$J_{u'} = \frac{\partial^2 S}{\partial I_u \partial I'} = 2 M n_v K_{u'}; \quad (B \cdot 13)$$

Using (B.10) and relations

$$\text{det} J = J_{11} J_{22} - J_{12}^2 = \frac{\partial (I_u; I')}{\partial (\varphi_1; \varphi_2)} (J_u J' - J_{u'}^2); \quad (B \cdot 14)$$

$$K' = \frac{1}{p a \sin}; \quad !_v = \frac{p}{m a \sin}; \quad (B \cdot 15)$$

one finally obtains

$$q_{EQ}^{(1)}(\mu) = \frac{1}{\mu_0} \operatorname{Re} \sum_{EQ}^X A_{EQ} \exp(ikL_{EQ} - i\frac{\pi}{2} L_{EQ}) ; \quad (B.16)$$

$$A_{EQ} = \frac{1}{2} \frac{\sin^3}{M n_v k R F_z} \operatorname{erf} Z_? ; Z_?^+ ; Z_1 ; Z_1^+ ; Z_2 ; Z_2^+ ; \quad (B.17)$$

where L_{EQ} represents length of the EQPO. The "triple" error function in Eq. (B.17) can be separated into the product of three standard error functions,

$$\operatorname{erf} Z_? ; Z_?^+ ; Z_1 ; Z_1^+ ; Z_2 ; Z_2^+ = \operatorname{erf} Z_? ; Z_?^+ \operatorname{erf} Z_1 ; Z_1^+ \operatorname{erf} Z_2 ; Z_2^+ \quad (B.18)$$

by taking the limits at the stationary points for all deformations, except for a small region near the spherical shape. In this way we obtain the simple results (3.30). The arguments of the error functions are given by (3.19) or (3.20) for Z_i ($i = 1; 2$) and

$$Z_? = \frac{S}{2} \frac{iJ_?^{EQ}}{2\pi} = \frac{\sim (k)^2}{16} \frac{S}{M n_v k a \sin} \frac{iF_z^{EQ}}{(\pi + 1) \det K^{EQ}} ; \quad (B.19)$$

The spherical limit is easily obtained by using the spherical action-angle variables $f ; r ; \varphi ; I ; I_r ; I_\varphi$. In these variables

$$A_{EQ} = \frac{1}{2} \frac{\sin^3}{M n_r k R F_z} \operatorname{erf} Z_? ; Z_?^+ ; Z ; Z^+ ; Z_r ; Z_r^+ ; \quad (B.20)$$

where $n_r = n_v$ for the equatorial-plane orbits with $(n_v; n_r)$, the invariant stability factor $F = F_z^{EQ}$ given by (B.9),

$$Z_? = \frac{V}{16 M n_r K^{EQ}} \frac{i F^{EQ}}{z - z_?} ; \quad Z_{f,g} = \frac{r}{i M n_r K_{f,g}^{EQ}} \frac{I_{f,g} - I_{f,g}^+}{z - z_{f,g}} ; \quad (B.21)$$

The quantities K^{EQ} and K_r^{EQ}

$$K_{f,g}^{EQ} = \frac{\partial^2 H}{\partial I_{f,g}^2} \bigg|_{EQ} ; \quad (B.22)$$

are the curvatures of the energy surface $H = H(I ; I_r ; I_\varphi)$ in the spherical coordinate system. In that system the maximum value of I_φ is equal to the absolute value of the classical angular momentum I_φ , $I_\varphi = I_\varphi^+$ being the maximum value of $|I_\varphi|$ and $I_\varphi = 0$. We note that for the diametric orbits the stationary points I_φ and I_φ^+ are

exactly zero and there are also specific integration limits in Eq. (B·20). In this case the internal integral over I_+ within a small region can be evaluated approximately as $2I_+$, and one obtains for the "triple" error function

$$\text{erf } Z_-; Z_-^+; Z_-^+; Z_+^+; Z_+; Z_+^+ \approx \frac{S}{M} \frac{4iF_z}{2n_r \sim K^{EQ}} = \frac{r}{2M} \frac{4iF_z kR}{2M} : \quad (\text{B} \cdot 23)$$

We used here the fact that, in the spherical limit $F_z \rightarrow 0$, the integral over Z_- can be approximated by the upper limit Z_-^+ given by Eq. (B·21). We omitted also the strong oscillating value of $\int_{-R}^R dz^2 e^{-z^2}$ at the upper limit since it vanishes after any small averaging over kR and equals 1 in this approximation. We also accounted for the fact that $K^{EQ} \rightarrow 1 = (pR)$ for the diameters; see Eq. (B·22) ($\beta = \beta_2$ for the diameters). Finally, the stability factor F_z is canceled and one obtains the Balian-Bloch result (3·33) for the contribution of the diametric orbits in the spherical cavity.³⁾

For all other EQPO one has the stationary points $I_+ = I_- \neq 0$ and I_+ is identical to its maximum value I_+ in the spherical limit. This is the reason why there is no next order ($1/kR$) corrections to the Balian-Bloch trace formula for the contribution of the planar orbits with $n_r = 3$. The latter comes from the spherical limit of the elliptic orbits in the meridian plane (3·16), see Ref. 9).

Appendix C

—— Separatrix ——

Like for the case of the turning points,^{39),41),(43)} we first expand the exponent phase in Eq. (3·6) with respect to I_u^0 :

$$S(I^0; I^0; t) = I^0 - I^0 - \omega = c_0^k + c_1^k x + c_2^k x^2 + c_3^k x^3 + \dots$$

$$c_0^k = \frac{k}{0} + \frac{k}{1} z + \frac{1}{3} z^3 : \quad (\text{C} \cdot 1)$$

Here

$$x = \frac{1}{\sim} \frac{I_u^0}{I_u^0} - \frac{I_u^0}{I_u^0} ; \quad (\text{C} \cdot 2)$$

$$c_0^k = \frac{1}{\sim} S(I^0; I^0; t) - I^0 - I^0 - \omega = \frac{1}{\sim} S(I^0; I^0; t) - \omega ; \quad (\text{C} \cdot 3)$$

$$c_1^k = \frac{\partial S}{\partial I_u^0} \omega_u = \frac{0}{u} - \frac{\omega_u}{u} \neq 0; \quad \frac{1}{1} \neq 1; \quad (\text{C} \cdot 4)$$

$$c_2^k = \frac{\sim}{2} \frac{\partial^2 S}{\partial I_u^{02}} = 2p M \sim K_u \neq 1; \quad \frac{1}{1} \neq 1; \quad (\text{C} \cdot 5)$$

$$c_3^k = \frac{\sim^3}{6} \frac{\partial^3 S}{\partial I_u^{03}} = \frac{2 \sim^3 \sim^2 M}{3(p^2)^2} \frac{\partial K_u}{\partial I_u} < 0; \quad k \neq 1; \quad (C.6)$$

where the superscript asterisk indicates the value at $I_u^0 = I_u^{\infty} = I_u$. The asymptotic behavior of the constants c_1^k near the separatrix $\gamma_1 = 1$ is found from

$$K_u \neq \frac{\log[(1 + \sin \gamma_1) = (1 - \sin \gamma_1)]}{(\gamma_1 - 1) \log^3(\gamma_1 - 1)}; \quad \gamma_1 \neq 1; \quad (C.7)$$

for $\gamma_1 \rightarrow 1$ formally, see (2.6),

$$\frac{\partial K_u}{\partial I_u} \neq \frac{2 \log[(1 + \sin \gamma_1) = (1 - \sin \gamma_1)]}{(\gamma_1 - 1) \log^2(\gamma_1 - 1)^2}; \quad \gamma_1 \neq 1; \quad (C.8)$$

The rightmost part of Eq. (C.1) is obtained by a linear transformation with some constants and γ_1 ,

$$x = z + \gamma_1; \quad \gamma_1 = 3c_3^k \sim^{1=3}; \quad \gamma_1 = c_2^k = (3c_3^k); \quad (C.9)$$

$$c_0^k = c_0 - c_1 c_2 = (3c_3) + 2c_2^3 = (27c_3^2) \sim^k; \quad c_1^k = c_1 - c_2^2 = (3c_3) \sim^k; \quad (C.10)$$

Near the stationary point for $\gamma_1 \neq 1$, one obtains $c_1^k \neq 0$ and $c_1^k \neq w^k$ with the positive quantity

$$w^k = \frac{c_2^2}{(3c_3)^{4=3}} \neq \frac{M \log[(1 + \sin \gamma_1) = (1 - \sin \gamma_1)] (\gamma_1 - 1)^{2=3}}{\sim \log(\gamma_1 - 1)}; \quad (C.11)$$

Using expansion (C.1) in Eq. (3.6) and taking the integral over γ_v^{∞} exactly (i.e., putting 2 for this integral), we obtain

$$g_{LD}^{(0)} = \frac{2}{2 \sim^2} \text{Re} \int_{\gamma_v^{\infty}}^{\gamma_v^{\infty}} d\gamma_v^{\infty} \int_{\gamma_v^{\infty}}^{\gamma_v^{\infty}} d\gamma_v^{\infty} \int_{\gamma_v^{\infty}}^{\gamma_v^{\infty}} d\gamma_v^{\infty} \frac{1}{j! v j} e^{i \gamma_v^{\infty} \sim^2} \frac{\gamma_v^{\infty} \overline{w^k}^h}{c_2^k} A i \gamma_v^{\infty} w^k; Z_k; Z_k^+ + i G i \gamma_v^{\infty} w^k; Z_k; Z_k^+ \sim^i$$

$$\sim^2 \text{Re} \int_{\gamma_v^{\infty}}^{\gamma_v^{\infty}} d\gamma_v^{\infty} \int_{\gamma_v^{\infty}}^{\gamma_v^{\infty}} d\gamma_v^{\infty} \frac{1}{j! v j} \frac{\gamma_v^{\infty} \overline{w^k}^h}{c_2^k} A i \gamma_v^{\infty} w^k + i G i \gamma_v^{\infty} w^k \sim^i e^{i \gamma_v^{\infty} \sim^2}; \quad (C.12)$$

where

$$Z_k = \frac{\gamma_v^{\infty} \overline{w^k}}{c_2^k}; \quad Z_k^+ = \frac{\gamma_v^{\infty} \overline{I_u^{(cr)}}}{\gamma_v^{\infty} \overline{w^k}} + \frac{\gamma_v^{\infty} \overline{w^k}}{c_2^k}; \quad (C.13)$$

$Ai(w; z_1; z_2)$ and $Gi(w; z_1; z_2)$ are the incomplete Airy and Gairy functions defined by

$$\frac{Ai(w; z_1; z_2)}{Gi(w; z_1; z_2)} = \frac{1}{z_1} \int_{z_1}^{z_2} dz \frac{\cos(wz + \frac{z^3}{3})}{\sin(wz + \frac{z^3}{3})}; \quad (C \cdot 14)$$

$Ai(w)$ and $Gi(w)$ are the corresponding standard complete functions, $I_u^{(cr)} = I_u(\frac{(cr)}{1}; \frac{(cr)}{1})$ is the "creeping" elliptic 2DPO value defined in section 2. In the second equation of (C ·12), we used the fact that for any finite deformation and large kR near the separatrix ($\epsilon_1 \rightarrow 1$)

$$\begin{aligned} z_k &\rightarrow 0; \\ z_k^+ &\rightarrow 4 \frac{M \log[(1 + \sin \epsilon_1) = (1 - \sin \epsilon_1)] p^{1=3}}{2(\epsilon_1 - 1)^2 \log^4(\epsilon_1 - 1)} \frac{p^{\frac{1}{2}}}{1} \frac{1}{1} \end{aligned} \quad (C \cdot 15)$$

Using an analogous expansion of the action ϕ_0^k in (C ·12) with respect to the angle ϕ_u to the third order and a linear transformation like (C ·9) one arrives at

$$\begin{aligned} q_{LD}^{(0)}(\epsilon) &= \frac{b}{2\epsilon_0^2 R} \operatorname{Re} \int_{\epsilon_0}^{\epsilon} d\epsilon \frac{1}{kR} \frac{w^k w^?}{\mathcal{P}_2^k c_2^? j} \\ &\quad \frac{h}{Ai(w^k + iGi(w^k; z_?; z_?^+)) + iGi(w^?; z_?; z_?^+)} \exp \left[\frac{i}{\sim} S(I^0; I^0; \epsilon) \right] \\ &\quad + \frac{2i}{3} \frac{h}{(w^k)^{3=2} + (w^?)^{3=2}} \frac{i}{2}; \end{aligned} \quad (C \cdot 16)$$

where

$$w^? = \frac{\mathcal{C}_2^2}{(3c_3)^{4=3}} > 0; \quad (C \cdot 17)$$

$$z_? = \frac{p}{w^?}; \quad z_?^+ = \frac{1=3}{2} 3c_3^2 + \frac{p}{w^?}; \quad (C \cdot 18)$$

$$c_2^? = \frac{1}{2\sim} J_u^?; \quad = \frac{\partial^2 S}{\partial \epsilon_u^2} + 2 \frac{\partial^2 S}{\partial \epsilon_u \partial \epsilon_u} + \frac{\partial^2 S}{\partial \epsilon_u^2} = \frac{F_{xy}^{LD}}{2MK_u}; \quad (C \cdot 19)$$

F_{xy}^{LD} is the stability factor for the long diameters,

$$F_{xy}^{LD} = 4 \sinh^2 M \operatorname{arccosh} 2^2 - 1; \quad (C \cdot 20)$$

$$\begin{aligned}
c_3^2 &= \frac{1}{6} \frac{\partial^3 S}{\partial u^3} + 3 \frac{\partial^3 S}{\partial u^2 \partial \varphi} + 3 \frac{\partial^3 S}{\partial u \partial \varphi^2} + \frac{\partial^3 S}{\partial \varphi^3} \\
&= \frac{1}{6} \frac{\partial J_u^2}{\partial u} + \frac{\partial J_u^2}{\partial \varphi} < 0;
\end{aligned} \tag{C 21}$$

Note that according to (C 19) the quantity c_2^2 approaches zero near the separatrix ($\varphi \rightarrow 1$) like in the caustic case. This is the reason why we apply the Maslov-Fedoryuk theory^{(39),(41),(43)} for the transformation of the integral over angle φ from (C 12) to (C 16). The remaining two integrals over the azimuthal variables (φ^0 and φ^0) can be calculated in a similar way as explained in the text.

Divergence of the curvature K , Eq. (B 13), for the long diameters ($\varphi \rightarrow 1$, $\varphi \rightarrow 0$) can be easily seen from the following expression valid for any polygon orbit having a vertex on the symmetry axis,

$$K = \frac{L_0 c}{2 n_v M} \sim \frac{2}{1 + \tan^2} \rightarrow 1; \tag{C 22}$$

where L_0 denotes the length of the side having a vertex at the pole, φ_0 the cylindrical coordinate of another end of this side, and φ the angle between this side and the symmetry axis. For the long diameters, $L_0 \rightarrow 2b$, $\varphi_0 \rightarrow 0$ and $\varphi \rightarrow 0$, so that $K \rightarrow 1$.

Appendix D

Derivation of the third-order term

D.1. Third-order curvatures

For the curvature $K_1^{(3)}$ which appears in the third-order terms in the expansion of the action $S \sim$ with respect to φ_1 , one obtains

$$K_1^{(3)} = \frac{1}{p} K_1^{(3)} = \frac{\partial^3 \mathcal{I}_v}{\partial \varphi_1^3} + \frac{n_u}{n_v} \frac{\partial^3 \mathcal{I}_u}{\partial \varphi_1^3}; \tag{D 1}$$

where

$$\begin{aligned}
\frac{\partial^3 \mathcal{I}_v}{\partial \varphi_1^3} &= \frac{1}{4z_+^3} \frac{\partial B_v}{\partial \varphi_1} + 6z_+ \frac{\partial z_+^2}{\partial \varphi_1} \frac{\partial^2 \mathcal{I}_v}{\partial \varphi_1^2}; \\
\frac{\partial^3 \mathcal{I}_u}{\partial \varphi_1^3} &= \frac{1}{2z_+^3} \frac{\partial B_u}{\partial \varphi_1} - 3z_+ \frac{\partial z_+^2}{\partial \varphi_1} \frac{\partial^2 \mathcal{I}_u}{\partial \varphi_1^2};
\end{aligned} \tag{D 2}$$

$$B_v = (\varphi'; k^2; k) - F(\varphi'; k) \mathcal{G}_k - \frac{\partial z_+^2}{\partial \varphi_1} F(\varphi'; k) + \frac{2z_+^2}{\varphi_1} \frac{\partial \varphi'}{\partial \varphi_1}; \tag{D 3}$$

$$\begin{aligned}
B_u &= (k^2; k) - F(k) \mathcal{G}_k - \frac{\partial z_+^2}{\partial \varphi_1} F(k); \\
\mathcal{G}_k &= \frac{z_+^2}{k^2} \frac{\partial k^2}{\partial \varphi_1} = \frac{1}{k^2} \frac{\partial z^2}{\partial \varphi_1} - \frac{\partial z_+^2}{\partial \varphi_1};
\end{aligned} \tag{D 4}$$

with the derivatives

$$\begin{aligned} \frac{\partial B_u}{\partial \epsilon_1} &= k \frac{\partial (k^2; k)}{\partial k} \frac{\partial F(k)}{\partial k} \frac{\partial_k^2}{2z_+^2} + (k^2; k) F(k) \frac{\partial_k}{z^2} \frac{\partial z^2}{\partial \epsilon_1} \\ &+ \frac{1}{k^2} \frac{\partial^2 z^2}{\partial \epsilon_1^2} \frac{\partial^2 z_+^2}{\partial \epsilon_1^2} k \frac{\partial F(k)}{\partial k} \frac{\partial_k}{2z_+^2} \frac{\partial z_+^2}{\partial \epsilon_1} \frac{\partial^2 z_+^2}{\partial \epsilon_1^2} F(k); \\ \frac{\partial^2 z^2}{\partial \epsilon_1^2} &= \frac{2 \epsilon_2}{[(\epsilon_1 - 1)^2 + 4 \epsilon_2]^3}; \end{aligned} \quad (D \cdot 5)$$

$$\begin{aligned} \frac{\partial B_v}{\partial \epsilon_1} &= \partial_k \frac{\partial ({}' ; k^2; k)}{\partial \epsilon_1} \frac{\partial F({}' ; k)}{\partial \epsilon_1} + 1 \frac{1}{z^2} \frac{\partial z^2}{\partial \epsilon_1} \frac{\partial^2 z_+^2}{\partial \epsilon_1^2} F({}' ; k) \\ &\frac{\partial z^2}{\partial \epsilon_1} \frac{\partial F({}' ; k)}{\partial \epsilon_1} + \frac{1}{\epsilon_1} \frac{\partial z_+^2}{\partial \epsilon_1} \frac{z_+^2}{\epsilon_1} \frac{\partial \epsilon_1'}{\partial \epsilon_1} + 2z_+^2 \frac{\partial^2 \epsilon_1'}{\partial \epsilon_1^2} : \end{aligned} \quad (D \cdot 6)$$

Here

$$\frac{\partial (k^2; k)}{\partial k} = \frac{k^2 \partial_k}{k_1^2 z_+^2} (k^2; k) + \frac{1}{2k^2} (E(k) - F(k)) ; \quad (D \cdot 7)$$

$$\frac{\partial F(k)}{\partial k} = \frac{1}{k} (k^2; k) - F(k) ; \quad (D \cdot 8)$$

$$\begin{aligned} \frac{\partial ({}' ; k^2; k)}{\partial \epsilon_1} &= \frac{1}{k_1^2} \frac{k^2 \partial_k}{z_+^2} ({}' ; k^2; k) + \frac{1}{2k^2} (E({}' ; k) - F({}' ; k)) \\ \frac{\sin(2')}{4 \epsilon_1^3} &= 1 + \frac{\epsilon_2'}{\epsilon_1^2} + \frac{\epsilon_1'}{\epsilon_1} \frac{1}{4 \epsilon_1^4} \left(4 \epsilon_2'^2 \cos(2') + k^2 \sin^2(2') \right) ; \end{aligned} \quad (D \cdot 9)$$

$$\frac{\partial F({}' ; k)}{\partial \epsilon_1} = \frac{\partial_k}{2z_+^2} ({}' ; k^2; k) - F({}' ; k) + \frac{1}{\epsilon_1} \frac{\partial \epsilon_1'}{\partial \epsilon_1} ; \quad (D \cdot 10)$$

$$\begin{aligned} \frac{\partial^2 \epsilon_1'}{\partial \epsilon_1^2} &= \frac{1}{\sin(2')} \left(\frac{1}{z_b^2 z^2} \frac{\partial^2 z^2}{\partial \epsilon_1^2} z_b^2 z_+^2 - \frac{\partial^2 z_+^2}{\partial \epsilon_1^2} z_b^2 z^2 \right. \\ &\left. + 2 \frac{\partial z^2}{\partial \epsilon_1} \frac{\partial z^2}{\partial \epsilon_1} z_b^2 z_+^2 - \frac{\partial z_+^2}{\partial \epsilon_1} z_b^2 z^2 - 2 \cos(2') \frac{\partial \epsilon_1'}{\partial \epsilon_1} \right) ; \end{aligned} \quad (D \cdot 11)$$

$$\frac{\partial^2 \epsilon_1'}{\partial \epsilon_1^2} = k^2 \frac{\partial_k}{z_+^2} \sin^2 \epsilon_1' + \sin(2') \frac{\partial \epsilon_1'}{\partial \epsilon_1} ; \quad (D \cdot 12)$$

D.2. Stationary phase method with third-order expansions

After the expansion of the action in the Poisson-sum trace formula (3.10) up to the second order with respect to z_2 and up to the third order with respect to z_1 , one obtains

$$g^{(2)}(\omega) = \frac{k^2}{4^2 R^2} \text{Re} \sum_{n_v R} \frac{L}{M_{n_v R}} \frac{\partial \Gamma_u}{\partial \epsilon_1} \exp(ikL) \frac{i}{2} \int_0^{z_2^+} dx \exp(ik M_{n_v} \tilde{K}_{22} z_2^2 + \frac{K_{12}}{K_{22}} (z_1 - z_1)) + i c_1 x + c_2 x^2 + c_3 x^3 \quad (D.13)$$

where

$$c_1 \neq 0; \quad c_2 = k M_{n_v} \frac{\det \tilde{K}}{K_{22}}; \quad c_3 = \frac{1}{3} k M_{n_v} \tilde{K}_1^{(3)}; \quad (D.14)$$

$$x = z_1 - z_1; \quad x = z_1 - z_1; \quad (D.15)$$

After transformation from z_2 to the new Z_2 variable,

$$Z_2 = \frac{q_1}{ik M_{n_v} \tilde{K}_{22} z_2^2 + \frac{K_{12}}{K_{22}} (z_1 - z_1)}; \quad (D.16)$$

and a linear transformation from x to z ,

$$x = q_1 z + q_2; \quad \text{with } q_1 = (3c_3)^{-1/3}; \quad q_2 = \frac{c_2}{3c_3}; \quad (D.17)$$

one obtains Eq. (3.15) with the ISPM 3 amplitude

$$A_{3D}^{(2)}(\omega) = \frac{L}{8 M_{n_v R} k M_{n_v} \tilde{K}_1^{(3)} z_1^{1/3}} \frac{\partial \Gamma_u}{\partial \epsilon_1} \exp \frac{2}{3} i \frac{3=2}{3} \text{erf} Z_2; Z_2^+ [A i(z; z_+) + i G i(z; z_+)] ; \quad (D.18)$$

Here Z_2 is defined by Eq. (3.20b) and

$$= (3c_3)^{-1/3} \frac{c_2^2}{3c_3} c_1; \quad z = \frac{x}{q_1} q_2; \quad (D.19)$$

In the limit $c_1 \neq 0$

$$= \frac{c_2^2}{(3c_3)^{4/3}} = \frac{(k M_{n_v})^{2/3} (\det \tilde{K} = K_{22})^2}{K_1^{(3)} 4^{1/3}}; \quad (D.20)$$

For finite curvatures far from the bifurcations, one can extend the limits of the Airy and Gairy functions ($z \neq 0$ and $z_+ \neq 1$) and obtains the complete Airy

$\text{Ai}(\cdot)$ and Gairy $\text{Gi}(\cdot)$ functions. Then, using the asymptotics of these functions for large $\eta / (kR)^{2/3}$ (large kR)

$$\frac{\text{Ai}(\cdot)}{\text{Gi}(\cdot)} \sim \frac{1}{\eta^{1/4}} \frac{\sin \frac{2}{3} \eta^{3/2}}{\cos \frac{2}{3} \eta^{3/2}} + \frac{1}{4} \quad (D \cdot 21)$$

and of the erf-function in Eq. (D ·18) one obtains the SSPM limit (3·21).